

Supporting information for

# Second sphere effects on H<sub>2</sub>O<sub>2</sub> activation by non-heme Fe<sup>II</sup> complexes: Role of a phenol group in the [H<sub>2</sub>O<sub>2</sub>]-dependent accumulation of Fe<sup>IV</sup>O vs Fe<sup>III</sup>OOH

Jean-Noël Rebilly,<sup>\*[a]</sup> Christian Herrero,<sup>[a]</sup> Katell Sénéchal-David,<sup>[a]</sup> Régis Guillot,<sup>[a]</sup> Tanya Inceoglu,<sup>[a]</sup> Hélène Maisonneuve,<sup>[a]</sup> and Frédéric Banse<sup>\*[a]</sup>

Université Paris-Saclay, CNRS, Institut de Chimie Moléculaire et des Matériaux d'Orsay (ICMMO), 91405 Orsay cedex, France

## Table of contents

I/ Materials and methods .....	1
II/ Ligand synthesis .....	3
II.1. Synthesis of 2,4-di-tert-butyl-6-(azidomethyl)phenol .....	3
II.2. Synthesis of L <sub>5</sub> <sup>PhOH</sup> .....	5
III/ Synthesis of complexes .....	7
III.1. [(L <sub>5</sub> <sup>PhOH</sup> )Fe <sup>II</sup> Cl <sub>2</sub> ] (1) .....	7
III.2. [(L <sub>5</sub> <sup>PhOH</sup> )Fe <sup>II</sup> Cl]PF <sub>6</sub> (2) .....	9
III.3. [(L <sub>5</sub> <sup>PhOH</sup> )Fe <sup>II</sup> (MeCN)](PF <sub>6</sub> ) <sub>2</sub> (3) .....	12
III.4. [(L <sub>5</sub> <sup>PhOH</sup> )Fe <sup>II</sup> (OTf)](OTf) (4) .....	15
III.5. Determination of the magnetic moment of the complexes by the Evans NMR method. ....	18
IV/ Reactivity studies .....	21
IV.1. Reaction of [(L <sub>5</sub> <sup>PhOH</sup> )Fe <sup>II</sup> (OTf)](OTf) (4) with PhIO. ....	21
IV.2. Reaction of [(L <sub>5</sub> <sup>PhOH</sup> )Fe <sup>II</sup> (OTf)](OTf) (4) with H <sub>2</sub> O <sub>2</sub> . ....	33

## I/ Materials and methods

Solvents and chemicals were of reagent grade and were distilled prior to use. H<sub>2</sub><sup>16</sup>O<sub>2</sub> 35% in water and H<sub>2</sub><sup>18</sup>O<sub>2</sub> 2% in H<sub>2</sub><sup>18</sup>O were used.

**ESI mass spectrometry** analyses were performed with a Bruker MicroTOFq spectrometer using a sodium formate calibrant. Solvents: Methanol rs HPLC LC/MS (Carlo-Erba), Acetonitrile HPLC (Carlo-Erba).

For ESI-MS characterization of Fe<sup>IV</sup>O intermediates, various solutions were prepared: a 10<sup>-4</sup>M solution of **4** in MeCN, a 1.3 x 10<sup>-4</sup>M solution of **PhIO** in MeCN/MeOH, a 2 x 10<sup>-4</sup>M solution of H<sub>2</sub><sup>16</sup>O<sub>2</sub> (or H<sub>2</sub><sup>18</sup>O<sub>2</sub>) in MeCN. A 1:1 v:v mixture of Fe<sup>II</sup> and oxidant solution was made directly in the syringe and immediately (continuously) injected in the spectrometer.

**NMR** spectra were recorded on Bruker 250 MHz, 300 MHz, and 360 MHz spectrometers.

**Cyclic Voltammetry** experiments were performed using an Autolab potentiostat and a conventional 3 electrodes device (C working electrode, SCE reference electrode, Pt counter electrode). The electrolyte salt (TBAPF<sub>6</sub>) was recrystallized and all the glassware was dried at 110°C before use. All cyclic voltammograms (CVs) were recorded under argon in acetonitrile solution containing 0.1 M Bu<sub>4</sub>NPF<sub>6</sub> at a scan rate of 0.1 V/s at 20°C. All potential values are referred to SCE.

**X-band EPR** spectra were recorded on frozen solutions using a Bruker Elexsys 500E spectrometer equipped with a Bruker ER 4116DM X band resonator, an Oxford Instrument continuous flow ESR 900 cryostat, and an Oxford ITC 503 temperature control system. Conditions: Microwave frequency = 9.63 GHz, microwave power = 1.0 mW, modulation amplitude = 8 Gauss, modulation frequency = 100 KHz, Gain = 50 db, temperature = 90 K. Spectral simulations were done using the Bruker software XSophe.

**X-ray diffraction** data for compounds [(L<sub>5</sub><sup>PhOH</sup>)Fe<sup>II</sup>(H<sub>2</sub>O)(OH)](PF<sub>6</sub>) & [(L<sub>5</sub><sup>PhOH</sup>)Fe<sup>II</sup>Cl](PF<sub>6</sub>) was collected by using a Kappa X8 APPEX II Bruker diffractometer with graphite-monochromated MoK $\alpha$  radiation ( $\lambda$  = 0.71073 Å). Crystals were mounted on a CryoLoop (Hampton Research) with Paratone-N (Hampton Research) as cryoprotectant and then flashfrozen in a nitrogen-gas stream at 100 K. For compounds, the temperature of the crystal was maintained at the selected value by means of a 700 series Cryostream cooling device to within an accuracy of  $\pm$ 1K. The data were corrected for Lorentz polarization, and absorption effects. The structures were solved by direct methods using SHELXS-97<sup>[1]</sup> and refined against F<sub>2</sub> by full-matrix least-squares techniques using SHELXL-2018<sup>[2]</sup> with anisotropic displacement parameters for all non-hydrogen atoms. Hydrogen atoms were located on a difference Fourier map and introduced into the calculations as a riding model with isotropic thermal parameters. All calculations were performed by using the Crystal Structure crystallographic software package WINGX.<sup>[3]</sup>

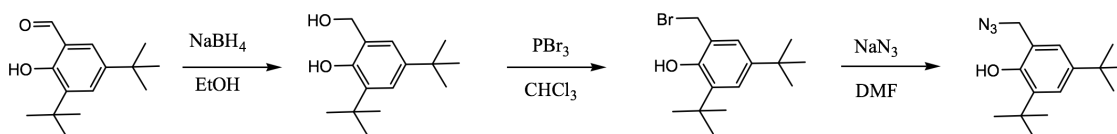
The crystal data collection and refinement parameters are given in Table S3.

CCDC 1992915-1992916 contains the supplementary crystallographic data for this paper. These data can be obtained free of charge from the Cambridge Crystallographic Data Centre via <http://www.ccdc.cam.ac.uk/Community/Requestastructure>.

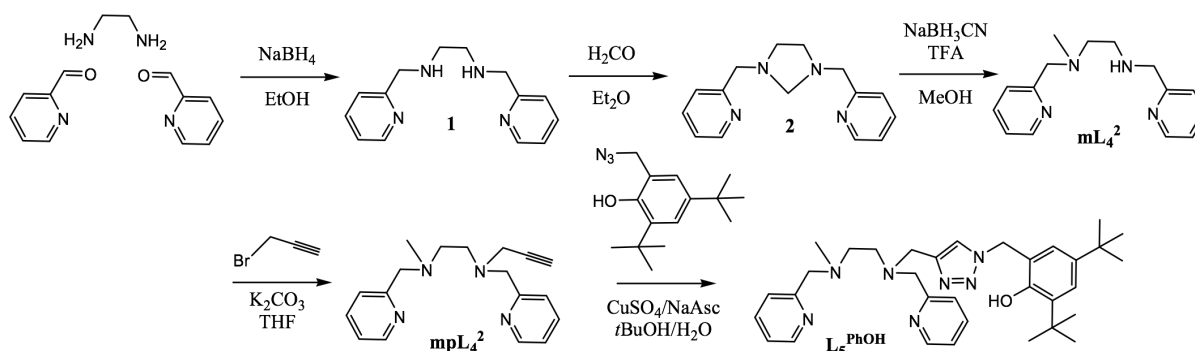
**Stopped Flow absorption spectrophotometry** was performed on a BioLogic SFM-4000 coupled to a J&M Tidas diode array spectrometer, with a two-syringes setup (one containing the iron complex, [Fe] = 2 mM, the other containing the oxidant). Experiments were at least triplicated for kinetic fits. Fits at 530 or 730 nm were performed using the BioKine software. Labeling experiments were carried out using the same setup, by simply changing the solvent of the complex and oxidant solutions: neat MeCN solvent was replaced by MeCN/H<sub>2</sub>O or MeCN/D<sub>2</sub>O 96:4 (v:v).

**UV-visible.** Electronic absorption spectra were recorded with a Varian Cary 60 spectrophotometer equipped with a Hellma immersion probe (1 cm optical pathlength) and fiber-optic cable. For low temperature experiments, a Thermo Haake CT90L cryostat was used.

## II/ Ligand synthesis



**Scheme S1.** Synthetic scheme of 2,4-di-tert-butyl-6-(azidomethyl)phenol



**Scheme S2.** Synthesis of  $L_5^{\text{PhOH}}$

2,4-di-tert-butyl-6-(hydroxymethyl)phenol and 2-(bromomethyl)-4,6-di-tert-butylphenol were synthesized according to previously reported methods.<sup>[4-5]</sup> Compounds **1**, **2**,  $mL_4^2$  and  $mpL_4^2$  were synthesized according to literature procedures.<sup>[6-8]</sup>

### II.1. Synthesis of 2,4-di-tert-butyl-6-(azidomethyl)phenol

2-(bromomethyl)-4,6-di-tert-butylphenol (506 mg, 1.7 mmol) was dissolved in 2 mL DMF. Sodium azide (220 mg, 3.4 mmol) was added and the solution was stirred overnight. Water (10 mL) was added, and the solution was extracted with diethyl ether (3 x 20 mL). The organic phase was washed with water (2 x 20 mL), dried over  $MgSO_4$ , filtered and evaporated to dryness. The product was isolated as a yellow oil (296 mg, 67%).

$^1H$  NMR (300K, 360 MHz,  $CDCl_3$ ).  $\delta$  (ppm) 1.29 (s, 9H, tBu), 1.42 (s, 9H, tBu), 4.43 (s, 2H,  $CH_2N_3$ ), 5.78 (s, 1H, OH), 6.99 (d, 1H,  $H_{Ar}$ ,  $J = 2.6$  Hz), 7.31 (d, 1H,  $H_{Ar}$ ,  $J = 2.6$  Hz).

IR.  $\nu_{N_3}$  2111  $cm^{-1}$ .

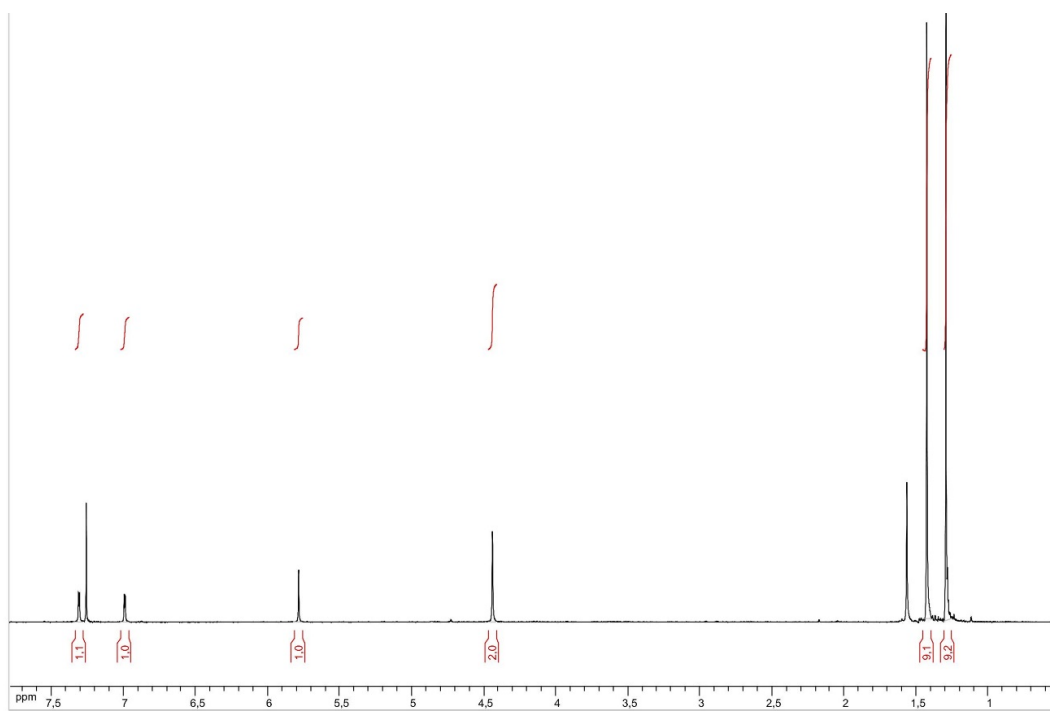


**Figure S1.** <sup>1</sup>H NMR spectrum (300K, 360 MHz, CDCl<sub>3</sub>) of 2,4-di-tert-butyl-6-(azidomethyl)phenol

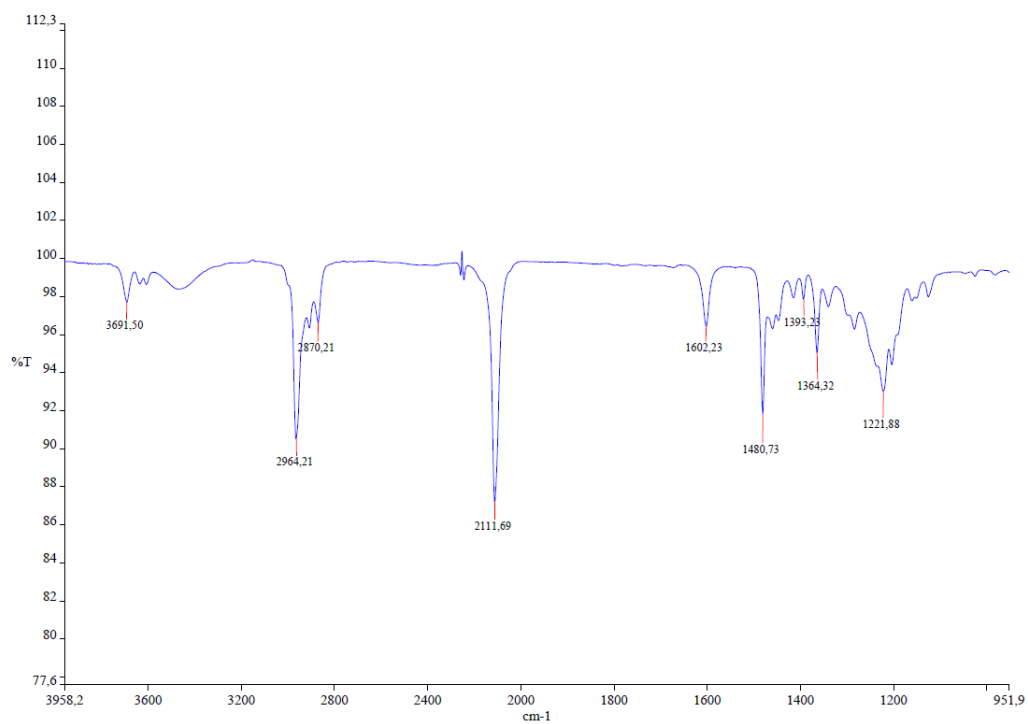
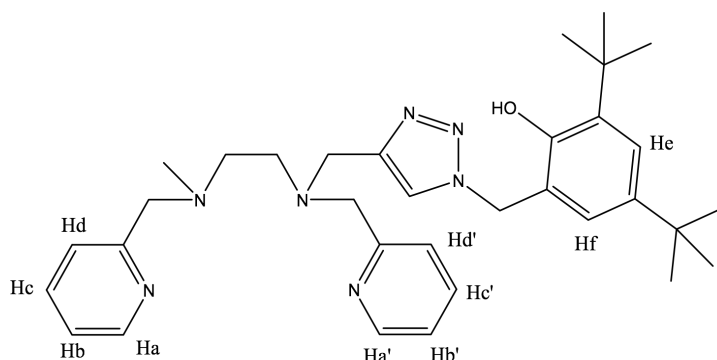


**Figure S2.** IR spectrum of 2,4-di-tert-butyl-6-(azidomethyl)phenol

## II.2. Synthesis of $L_5^{PhOH}$



**Scheme S3.** Proton designation in  $L_5^{PhOH}$

$mpL_4^2$  (100 mg, 0.34 mmol), 2,4-di-tert-butyl-6-(azidomethyl)phenol (89 mg, 0.34 mmol), and  $ZnSO_4 \cdot 7H_2O$  (98 mg, 0.34 mmol) were dissolved in  $tBuOH/H_2O$  1:1 (6.5 mL) in a round bottom flask equipped with a condenser. After 10 minutes stirring, sodium ascorbate was added (33 mg, 0.17 mmol) and the mixture was degassed and placed under argon.  $CuSO_4 \cdot 5H_2O$  (4.3 mg, 0.017 mmol) was added and the mixture was heated to reflux overnight. The reaction mixture was cooled down. EDTA (250 mg, 1.26 mmol) was added. The mixture was diluted with  $CH_2Cl_2$  and stirred under air for 3 hours. The aqueous phase was extracted with  $CH_2Cl_2$  (3 x 30 mL). The organic phases were washed with brine (10 mL), dried over  $Na_2SO_4$ , filtered and evaporated to dryness to give an oil. The product was purified by chromatography on basic alumina (Akt. III), eluting first with  $CH_2Cl_2$  and then  $CH_2Cl_2$  / MeOH (95:5). The product ( $R_f = 0.45$ ,  $CH_2Cl_2$  / MeOH 95:5) was isolated as an oil that turns into foam under vacuum (127 mg, 67%)

**$^1H$  NMR (360 MHz, 300 K,  $CDCl_3$ ).**  $\delta$  (ppm) 8.46 (2H, t,  $J = 6.2$  Hz, Ha, Ha'), 8.20 (1H, br, HOH), 7.69 (1H, s, HTria), 7.56 (2H, tt,  $J = 7.5$  Hz,  $J' = 2.3$  Hz, Hc, Hc'), 7.41 (1H, d,  $J = 8.2$  Hz, Hd), 7.34 (1H, d,  $J = 8.2$  Hz, Hd'), 7.33 (1H, d,  $J = 2.3$  Hz, He), 7.08 (2H, m, Hb, Hb') 7.05 (1H, d,  $J = 2.3$  Hz, Hf), 5.39 (2H, s,  $CH_2PhOH$ ), 2.77 (2H, s,  $CH_2py$ ), 3.74 (2H, s,  $CH_2py$ ), 3.61 (2H, s,  $CH_2Tria$ ), 2.69 (2H, t,  $J = 6.2$  Hz, N- $CH_2-CH_2-N$ ), 2.62 (2H, t,  $J = 6.2$  Hz, N- $CH_2-CH_2-N$ ), 2.17 (3H, s, N-Me), 1.39 (9H, s, tBu), 1.26 (9H, s, tBu).

**$^{13}C$  NMR (90 MHz, 300 K,  $CDCl_3$ ).**  $\delta$  (ppm) 29.89, 31.57, 34.29, 35.15, 42.78, 48.97, 51.61, 51.75, 55.45, 60.12, 64.04, 122.04, 122.34, 123.27, 123.33, 123.50, 124.93, 125.41, 136.52, 138.79, 142.75, 144.81, 148.91, 148.95, 152.22, 159.11, 159.22.

**HR-ESI-MS.**  $m/z = 556.3743$  (calcd. for  $[L_5^{PhOH} + H^+] = 556.3758$ , error = 1.5 ppm),  $m/z = 578.3559$  (calcd. for  $[L_5^{PhOH} + Na^+] = 578.3559$ , error = 1.8 ppm)

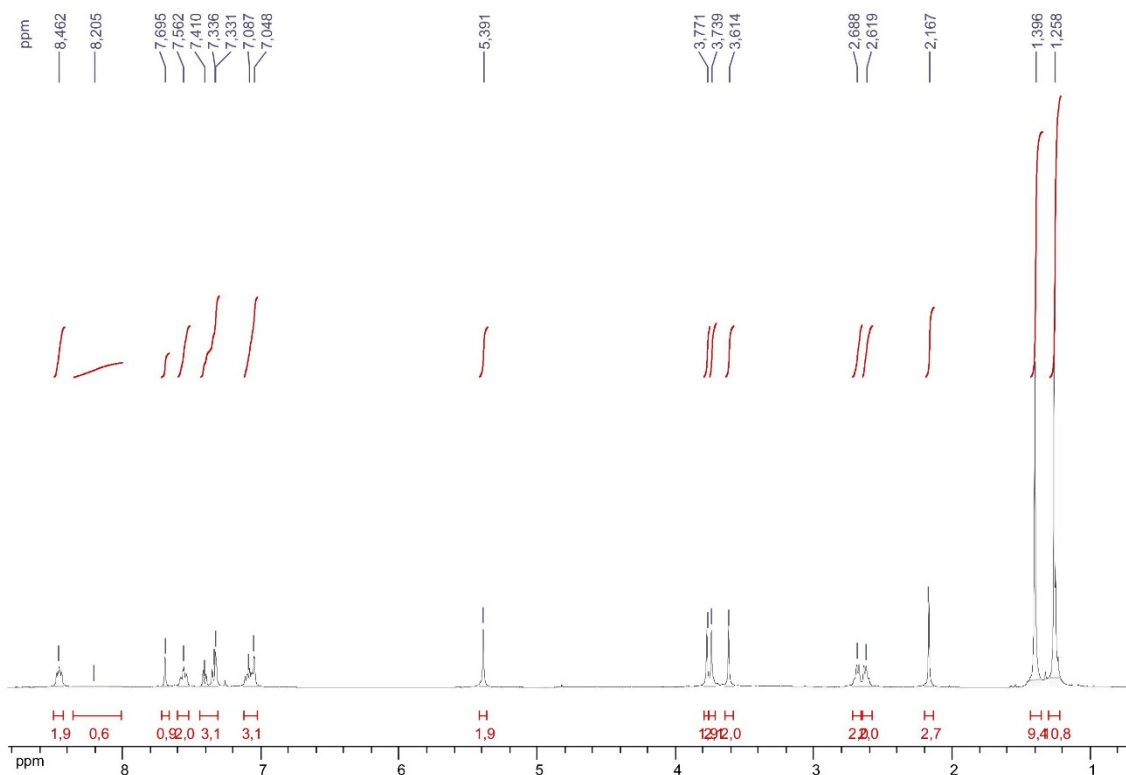


Figure S3.  $^1\text{H}$  NMR spectrum (360 MHz, 300 K,  $\text{CDCl}_3$ ) of  $\text{L}_5^{\text{PhOH}}$

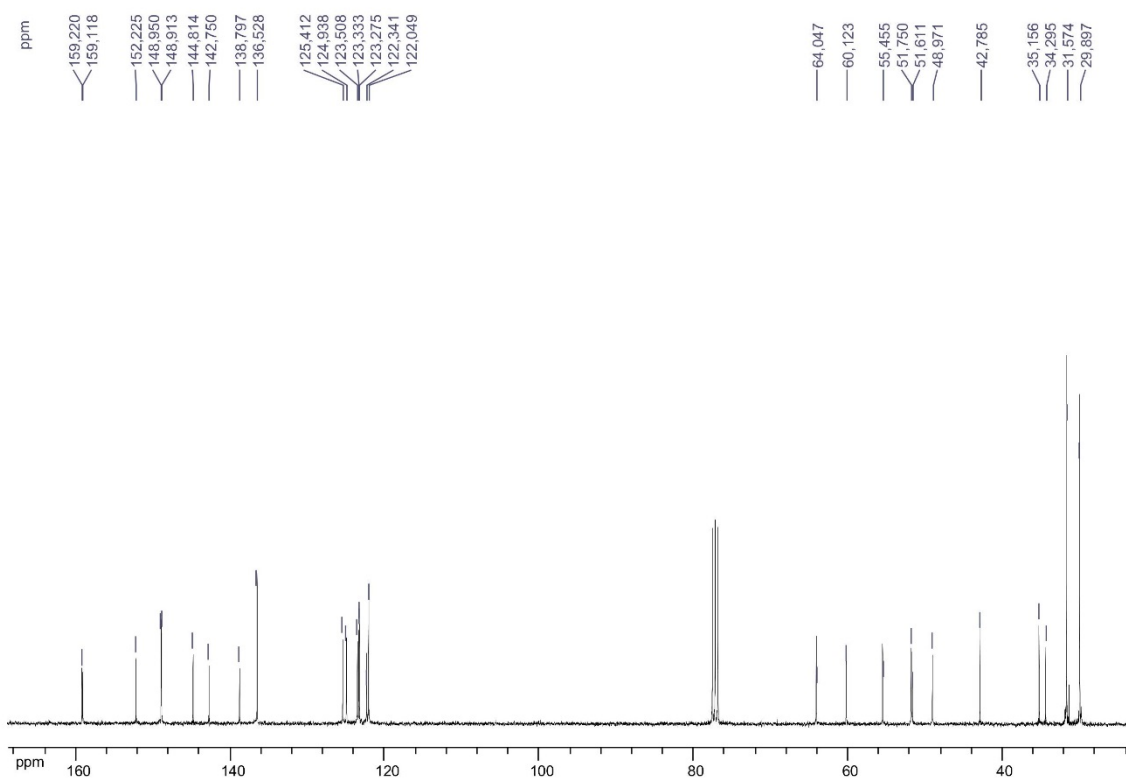
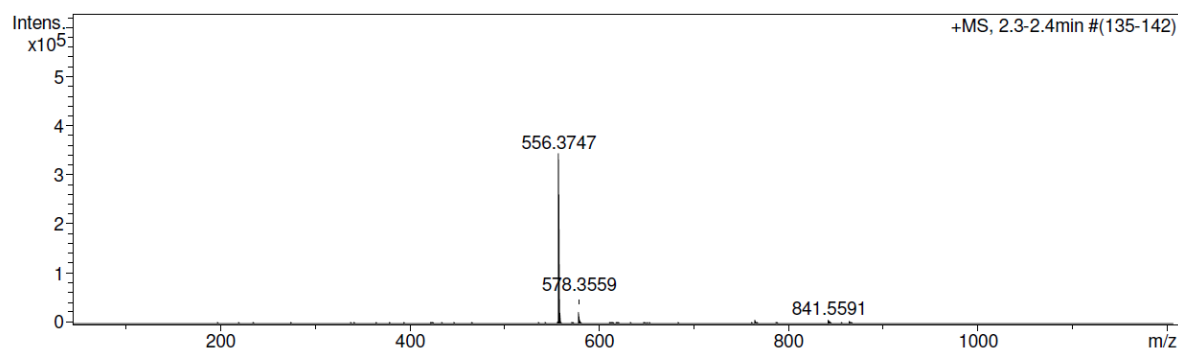
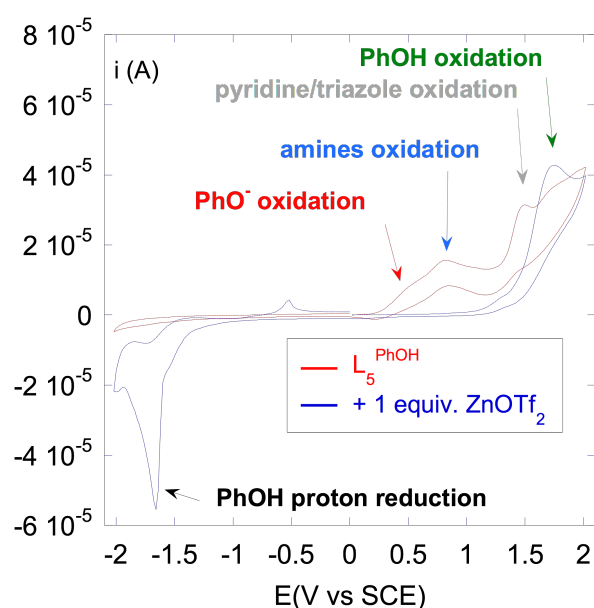


Figure S4.  $^{13}\text{C}$  NMR spectrum (90 MHz, 300 K,  $\text{CDCl}_3$ ) of  $\text{L}_5^{\text{PhOH}}$



**Figure S5.** HR-ESI-MS spectrum of  $L_5^{\text{PhOH}}$ .  $m/z = 556.3743$  (calcd. for  $[L_5^{\text{PhOH}} + \text{H}^+] = 556.3758$ , error = 1.5 ppm),  $m/z = 578.3559$  (calcd. for  $[L_5^{\text{PhOH}} + \text{Na}^+] = 578.3559$ , error = 1.8 ppm)



**Figure S6.** CV of  $L_5^{\text{PhOH}}$  (2 mM in MeCN,  $\text{NBu}_4\text{PF}_6$  0.1M) before (red) and after (blue) addition of 1 equiv.  $\text{Zn}(\text{OTf})_2$ .

The initial CV displays oxidation waves ascribed to the different groups of the ligand: phenol ( $E_p^a = 1.77$  V), pyridines/triazole ( $E_p^a = 1.50$  V), tertiary amines ( $E_p^a = 0.82$  V), phenolate ( $E_p^a = 0.45$  V). After addition of  $\text{Zn}(\text{OTf})_2$ , all these oxidation waves vanish, indicating metal binding of the corresponding groups, except for the phenol one, which indicates it is not bound and protonated. This is confirmed by the reduction wave at  $E_p^c = -1.65$  V, ascribed to the reduction of the phenol proton.

### III/ Synthesis of complexes

#### III.1. $[(L_5^{\text{PhOH}})\text{Fe}^{\text{II}}\text{Cl}_2]$ (1)

$L_5^{\text{PhOH}}$  (142 mg, 0.25 mmol) was dissolved in 3 mL MeCN in a glovebox and was added to a solution of  $\text{FeCl}_2 \cdot 2\text{H}_2\text{O}$  (41.4 mg, 0.25 mmol) in 2 mL MeCN. The solution turns yellowish-green. After 3 days

stirring, the product was isolated as a yellow precipitate, which was filtered, and washed with 2 mL MeCN (55%).

**HR-ESI-MS** (MeOH).  $m/z = 656.2977$  (calcd. for  $[(LH)Fe^{II}(\text{formate})]^+ = 656.3007$ , error = 4.4 ppm),  $m/z = 673.3371$  (calcd. for  $[(LH)Fe^{III}(\text{OMe})_2]^+ = 673.3398$ , error = 4.0 ppm).  $LH = L_5^{\text{PhOH}}$ , sodium formate is used for calibration.

**CV.** Mixture of species in solution,  $[(N_4)Fe^{II}Cl_2]$  ( $E_p^a = 0.27$  V),  $[(N_5)Fe^{II}(Cl)]^+$  ( $E_p^a = 0.58$  V), and  $[(N_5)Fe^{II}(\text{MeCN})]^{2+}$  ( $E_p^a = 1.05$  V). Oxidation waves of dangling di-tert-butylphenol ( $E_p^a = 1.63$  V, determined by comparison with the  $Zn^{II}$  complex, Figure S6), and triazole ( $E_p^a = 1.50$  V).

**UV-vis.** (MeOH, 300 K) 375 nm ( $\epsilon = 1100 \text{ L}\cdot\text{mol}^{-1}\cdot\text{cm}^{-1}$ ) MLCT; 319 nm ( $\epsilon = 1100 \text{ L}\cdot\text{mol}^{-1}\cdot\text{cm}^{-1}$ ); 282 nm ( $\epsilon = 3100 \text{ L}\cdot\text{mol}^{-1}\cdot\text{cm}^{-1}$ )  $\pi-\pi^*$  phenol; 260 nm ( $\epsilon = 7700 \text{ L}\cdot\text{mol}^{-1}\cdot\text{cm}^{-1}$ )  $\pi-\pi^*$ . The  $Fe^{II} \rightarrow py$  MLCT at 375 nm ( $\epsilon = 1100 \text{ L}\cdot\text{mol}^{-1}\cdot\text{cm}^{-1}$ ) is in agreement with predominantly high spin species, expected for anion bound complexes (low  $\epsilon$ ).

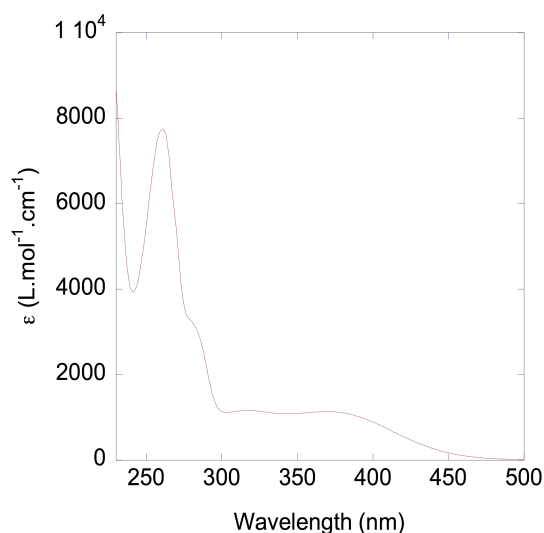


**Figure S7.** UV-vis spectrum of  $[(L_5^{\text{PhOH}})Fe^{II}Cl_2]$  in MeOH, 300 K. 375 nm ( $\epsilon = 1100 \text{ L}\cdot\text{mol}^{-1}\cdot\text{cm}^{-1}$ ) MLCT; 319 nm ( $\epsilon = 1100 \text{ L}\cdot\text{mol}^{-1}\cdot\text{cm}^{-1}$ ); 282 nm ( $\epsilon = 3100 \text{ L}\cdot\text{mol}^{-1}\cdot\text{cm}^{-1}$ )  $\pi-\pi^*$  phenol; 260 nm ( $\epsilon = 7700 \text{ L}\cdot\text{mol}^{-1}\cdot\text{cm}^{-1}$ )  $\pi-\pi^*$ .

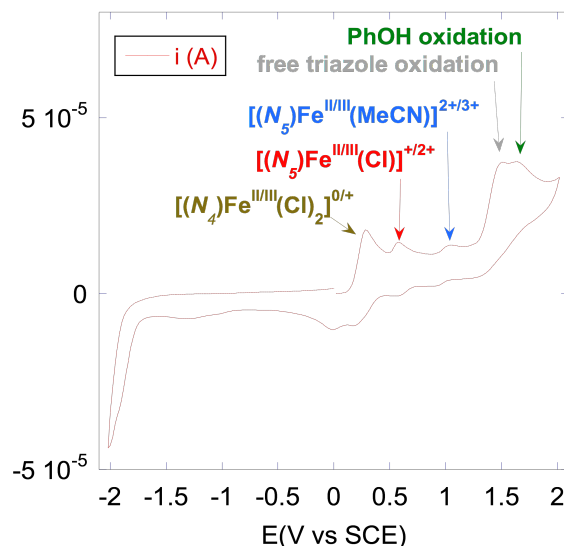


**Figure S8.** CV of  $[(L_5^{\text{PhOH}})\text{Fe}^{\text{II}}\text{Cl}_2]$  (2 mM in MeCN,  $\text{NBu}_4\text{PF}_6$  0.1M).

The CV displays the signatures of the couples  $[(N_5)\text{Fe}^{\text{III/II}}(\text{MeCN})]^{2+/3+}$  ( $E_p^a = 1.05$  V,  $E_p^c = 0.93$  V),  $[(N_5)\text{Fe}^{\text{III/II}}\text{Cl}]^{+/2+}$  ( $E_p^a = 0.58$  V,  $E_p^c = 0.52$  V),  $[(N_4)\text{Fe}^{\text{III/II}}\text{Cl}_2]^{0/+}$  ( $E_p^a = 0.27$  V,  $E_p^c = 0.19$  V, and of the pendant moieties of the ligand (phenol oxidation at  $E_p^a = 1.63$  V, triazole oxidation at  $E_p^a = 1.50$  V).

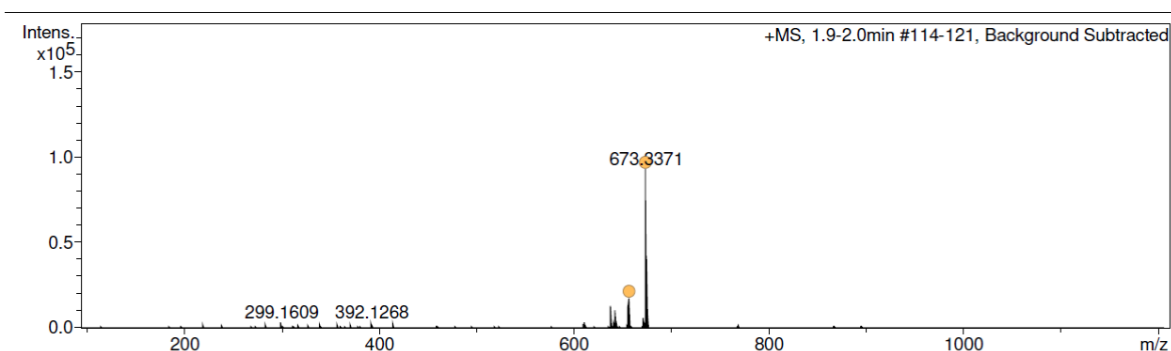


**Figure S9.** HR-ESI-MS spectrum (MeOH) of  $[(L_5^{\text{PhOH}})\text{Fe}^{\text{II}}\text{Cl}_2]$ .  $m/z = 656.2977$  (calcd. for  $[(L_5^{\text{PhOH}})\text{Fe}^{\text{II}}(\text{formate})]^+ = 656.3007$ , error = 4.4 ppm),  $m/z = 673.3371$  (calcd. for  $[(L_5^{\text{PhOH}})\text{Fe}^{\text{III}}(\text{OMe})_2]^+ = 673.3398$ , error = 4.0 ppm). NB: sodium formate is used for calibration.

### III.2. $[(L_5^{\text{PhOH}})\text{Fe}^{\text{II}}\text{Cl}]\text{PF}_6$ (**2**)

In a glovebox,  $[(L_5^{\text{PhOH}})\text{Fe}^{\text{II}}\text{Cl}_2]$  (60 mg, 0.09 mmol) was suspended in 1 mL MeCN.  $\text{AgPF}_6$  (22 mg, 0.09 mmol) in 1 mL MeCN was added resulting in a colour change of the precipitate from yellow to white (formation of a white  $\text{AgCl}$  precipitate). The solution was stirred for 1 hours and then filtered. The filtrate was evaporated to dryness. The residue was taken up in 1 mL  $\text{CH}_2\text{Cl}_2$ . The complex was precipitated as a yellow powder by addition of pentane (49 mg, 71%).

Crystals suitable for X-ray diffraction were obtained by slow diffusion of  $t\text{BuOMe}$  into a methanolic solution of the complex.

**UV-vis** (MeCN, 300 K). 385 nm ( $\epsilon = 1100 \text{ L}\cdot\text{mol}^{-1}\cdot\text{cm}^{-1}$ ) MLCT ; 315 nm ( $\epsilon = 1400 \text{ L}\cdot\text{mol}^{-1}\cdot\text{cm}^{-1}$ ); 283 nm ( $\epsilon = 2900 \text{ L}\cdot\text{mol}^{-1}\cdot\text{cm}^{-1}$ )  $\pi$ - $\pi^*$  phenol; 260 nm ( $\epsilon = 5600 \text{ L}\cdot\text{mol}^{-1}\cdot\text{cm}^{-1}$ )  $\pi$ - $\pi^*$

**CV** (2 mM in MeCN, WE: GC; CR: Pt; Ref: SCE;  $\text{NBu}_4\text{PF}_6$  0.1M).  $[(N_5)\text{Fe}^{\text{II/III}}(\text{MeCN})]^{2+/3+}$  ( $E_p^a = 1.03 \text{ V}$ ,  $E_p^c = 0.91 \text{ V}$ ),  $[(N_5)\text{Fe}^{\text{II/III}}\text{Cl}]^{+/2+}$  ( $E_p^a = 0.64 \text{ V}$ ,  $E_p^c = 0.59 \text{ V}$ ),  $[(N_4)\text{Fe}^{\text{II/III}}\text{Cl}]^{0/+}$  ( $E_p^c = 0.28 \text{ V}$ ), phenol oxidation at  $E_p^a = 1.63 \text{ V}$ .

**HR-ESI-MS** (MeOH).  $m/z = 646.2776$  (calcd. for  $[(\text{LH})\text{FeCl}]^+ = 646.2719$ , error = 1.1 ppm),  $m/z = 656.3024$  (calcd. for  $[(\text{LH})\text{Fe}^{\text{II}}(\text{formate})]^+ = 656.3003$ , error = 3.2 ppm). LH =  $\text{L}_5^{\text{PhOH}}$ .

**Magnetic properties in  $\text{CD}_3\text{CN}$  solution (Evans method).**  $[(\text{L}_5^{\text{PhOH}})\text{Fe}^{\text{II}}\text{Cl}]\text{PF}_6$  :  $\mu_{\text{eff}} = 5.058 \mu_{\text{B}}$  (98% HS)

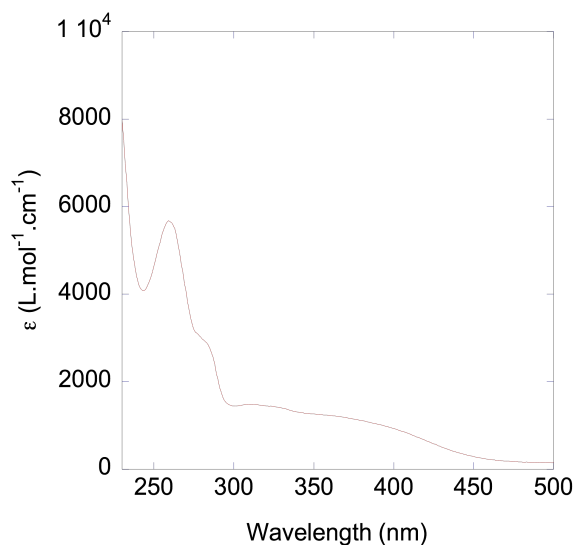


**Figure S10.** UV-vis spectrum of  $[(\text{L}_5^{\text{PhOH}})\text{Fe}^{\text{II}}\text{Cl}]\text{PF}_6$  in MeCN, 300 K. 385 nm ( $\epsilon = 1100 \text{ L}\cdot\text{mol}^{-1}\cdot\text{cm}^{-1}$ ) MLCT; 315 nm ( $\epsilon = 1400 \text{ L}\cdot\text{mol}^{-1}\cdot\text{cm}^{-1}$ ); 283 nm ( $\epsilon = 2900 \text{ L}\cdot\text{mol}^{-1}\cdot\text{cm}^{-1}$ )  $\pi$ - $\pi^*$  phenol; 260 nm ( $\epsilon = 5600 \text{ L}\cdot\text{mol}^{-1}\cdot\text{cm}^{-1}$ )  $\pi$ - $\pi^*$ .

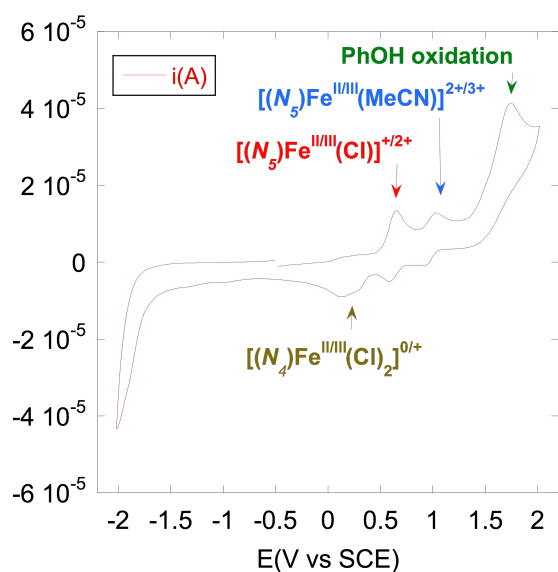


**Figure S11.** CV of  $[(L_5^{\text{PhOH}})\text{Fe}^{\text{II}}\text{Cl}](\text{PF}_6)$  (2 mM in MeCN,  $\text{NBu}_4\text{PF}_6$  0.1M). The CV displays the signatures of the couples  $[(N_5)\text{Fe}^{\text{II/III}}(\text{MeCN})]^{2+/3+}$  ( $E_p^a = 1.03$  V,  $E_p^c = 0.91$  V),  $[(N_5)\text{Fe}^{\text{II/III}}\text{Cl}]^{+/2+}$  ( $E_p^a = 0.64$  V,  $E_p^c = 0.59$  V),  $[(N_4)\text{Fe}^{\text{II/III}}\text{Cl}_2]^{0/+}$  ( $E_p^c = 0.28$  V), and of the pendant moieties of the ligand (phenol oxidation at  $E_p^a = 1.63$  V).

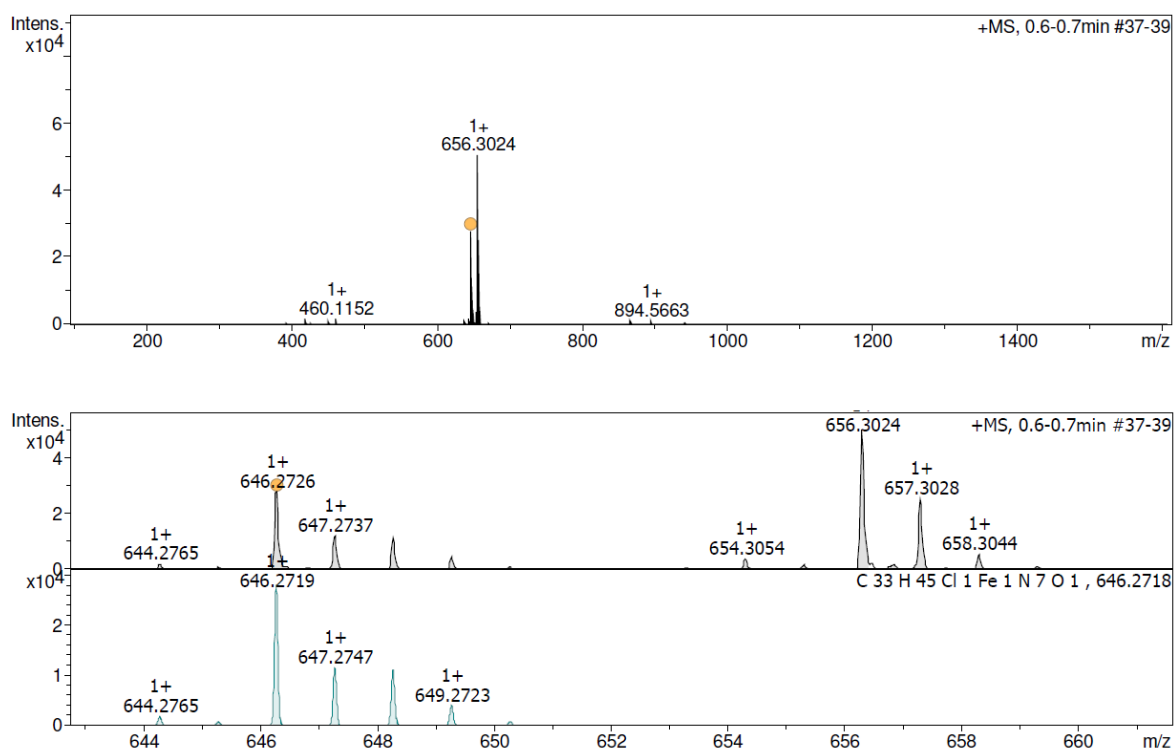


**Figure S12.** HR-ESI-MS spectrum of  $[(L_5^{\text{PhOH}})\text{Fe}^{\text{II}}\text{Cl}]\text{PF}_6$ .  $m/z = 646.2776$  (calcd. for  $[(L_5^{\text{PhOH}})\text{FeCl}]^+ = 646.2719$ , error = 1.1 ppm),  $m/z = 656.3024$  (calcd. for  $[(L_5^{\text{PhOH}})\text{Fe}^{\text{II}}(\text{formate})]^+ = 656.3003$ , error = 3.2 ppm).

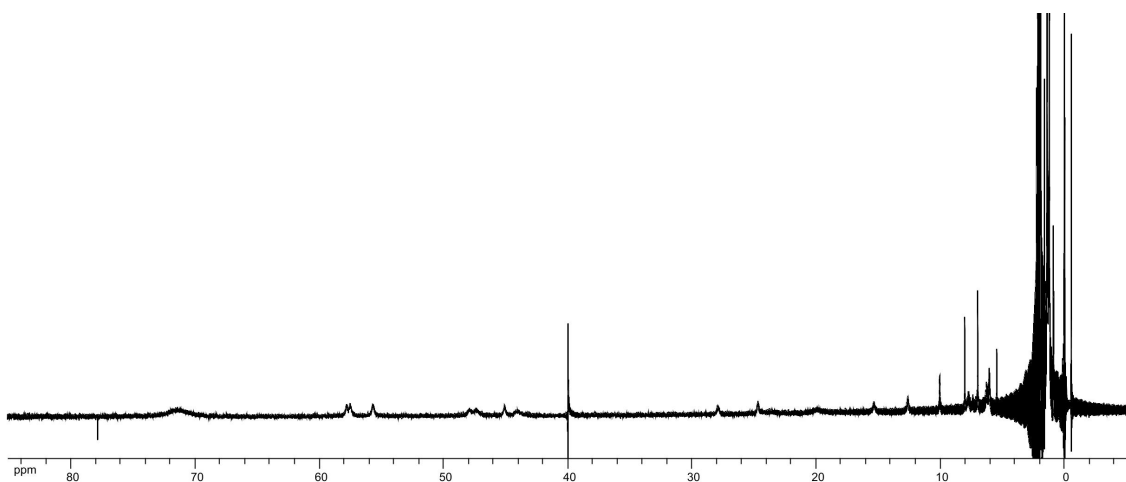


**Figure S13.**  $^1\text{H}$  NMR spectrum ( $\text{CD}_3\text{CN}$ , 360 MHz, 300 K) of  $[(\text{L}_5^{\text{PhOH}})\text{Fe}^{\text{II}}(\text{Cl})]\text{PF}_6$ .

### III.3. $[(\text{L}_5^{\text{PhOH}})\text{Fe}^{\text{II}}(\text{MeCN})](\text{PF}_6)_2$ (**3**)

In a glovebox,  $[(\text{L}_5^{\text{PhOH}})\text{Fe}^{\text{II}}\text{Cl}_2]$  (102 mg, 0.15 mmol) was suspended in 2 mL MeCN.  $\text{AgPF}_6$  (75.7 mg, 0.30 mmol) in 2 mL MeCN was added resulting in a colour change from yellow to dark brown, along with the formation of a white  $\text{AgCl}$  precipitate. The solution was stirred overnight and then filtered. The filtrate was evaporated to dryness. The residue was taken up in 1 mL MeOH, the solution turned yellow and was added dropwise on an excess of *tert*-butyl-methyl-ether. The precipitate was isolated and dried under vacuum (74%).

Slow diffusion of *t*-BuOMe into a methanolic solution of the complex gave crystals suitable for X-ray diffraction that corresponded to a rearranged complex  $[(\text{L}_5^{\text{PhOH}})\text{Fe}^{\text{II}}(\text{H}_2\text{O})(\text{OH})](\text{PF}_6)$ .

**UV-vis** 374 nm ( $\epsilon = 2800 \text{ L}\cdot\text{mol}^{-1}\cdot\text{cm}^{-1}$ ) MLCT; 321 nm ( $\epsilon = 1800 \text{ L}\cdot\text{mol}^{-1}\cdot\text{cm}^{-1}$ ); 284 nm ( $\epsilon = 3100 \text{ L}\cdot\text{mol}^{-1}\cdot\text{cm}^{-1}$ )  $\pi$ - $\pi^*$  phenol; 256 nm ( $\epsilon = 8300 \text{ L}\cdot\text{mol}^{-1}\cdot\text{cm}^{-1}$ )  $\pi$ - $\pi^*$ . The increase in the MLCT extinction coefficient, with respect to (1) and (2) is indicative of a more pronounced low spin character, in line with the predominant  $[(\text{N}_5)\text{Fe}^{\text{II}}(\text{MeCN})]^{2+}$  environment species.

**CV** (2 mM in MeCN, WE: GC; CR: Pt; Ref: SCE;  $\text{NBu}_4\text{PF}_6$  0.1M).  $[(\text{N}_5)\text{Fe}^{\text{II/III}}(\text{MeCN})]^{2+/3+}$  ( $E_p^a = 0.99 \text{ V}$ ,  $E_p^c = 0.81 \text{ V}$ , broad),  $[(\text{N}_4)\text{Fe}^{\text{II/III}}(\text{MeCN})(\text{OH})]^{+/2+}$  ( $E_p^a = 0.82 \text{ V}$ ,  $E_p^c = 0.81 \text{ V}$ , broad),  $[(\text{N}_4)\text{Fe}^{\text{II/III}}(\text{OH})_2]^{0/+}$  ( $E_p^c = 0.28 \text{ V}$ ), and of the pendant moieties of the ligand (phenol oxidation at  $E_p^a = 1.63 \text{ V}$ ).

**HR-ESI-MS** (MeOH). LH =  $\text{L}_5^{\text{PhOH}}$ .  $m/z = 656.3001$  (calcd. for  $[(\text{L}_5^{\text{PhOH}})\text{Fe}^{\text{II}}(\text{formate})]^+$  = 656.3007, error = 0.9 ppm),  $m/z = 673.3391$  (calcd. for  $[(\text{L}_5^{\text{PhOH}})\text{Fe}^{\text{III}}(\text{OMe})_2]^+$  = 673.3398, error = 1.0 ppm).

**Magnetic properties in  $\text{CD}_3\text{CN}$  solution (Evans method).**  $[(\text{L}_5^{\text{PhOH}})\text{Fe}^{\text{II}}(\text{MeCN})](\text{PF}_6)_2$  (**3**),  $\mu_{\text{eff}} = 3.193 \mu_B$  (62% HS).

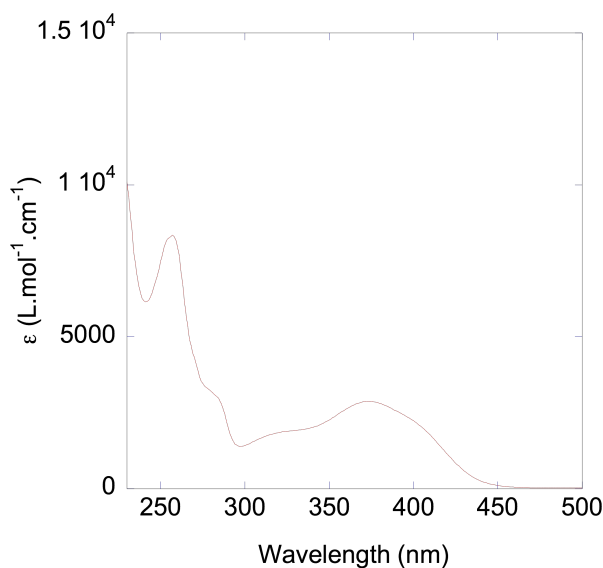


**Figure S14.** UV-vis spectrum of  $[(L_5^{\text{PhOH}})\text{Fe}^{\text{II}}(\text{MeCN})](\text{PF}_6)_2$  in MeCN, 300 K. MLCT 374 nm ( $\epsilon = 2800 \text{ L.mol}^{-1}.\text{cm}^{-1}$ );  $\text{Fe}^{\text{II}} \rightarrow \text{py}$ ; 321 nm ( $\epsilon = 1800 \text{ L.mol}^{-1}.\text{cm}^{-1}$ ); 284 nm ( $\epsilon = 3100 \text{ L.mol}^{-1}.\text{cm}^{-1}$ )  $\pi-\pi^*$  phenol; 256 nm ( $\epsilon = 8300 \text{ L.mol}^{-1}.\text{cm}^{-1}$ )  $\pi-\pi^*$ .

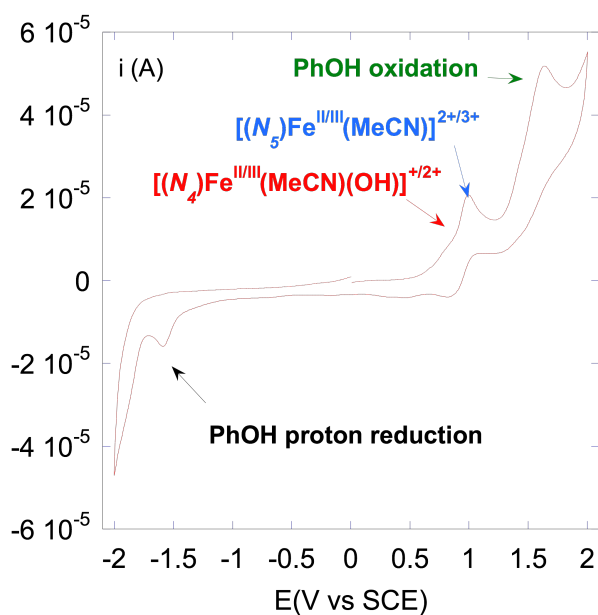


**Figure S15.** CV of  $[(L_5^{\text{PhOH}})\text{Fe}^{\text{II}}(\text{MeCN})](\text{PF}_6)_2$  (2 mM in MeCN,  $\text{NBu}_4\text{PF}_6$  0.1M).

The CV displays the signatures of the couples  $[(N_5)\text{Fe}^{\text{II/III}}(\text{MeCN})]^{2+/3+}$  ( $E_p^a = 0.99 \text{ V}$ ,  $E_p^c = 0.81 \text{ V}$ , broad),  $[(N_4)\text{Fe}^{\text{II/III}}(\text{MeCN})(\text{OH})]^{+/2+}$  ( $E_p^a = 0.82 \text{ V}$ ,  $E_p^c = 0.81 \text{ V}$ , broad),  $[(N_4)\text{Fe}^{\text{II/III}}(\text{OH})_2]^{0/+}$  ( $E_p^c = 0.28 \text{ V}$ ), and of the pendant moieties of the ligand (phenol oxidation at  $E_p^a = 1.63 \text{ V}$ ).

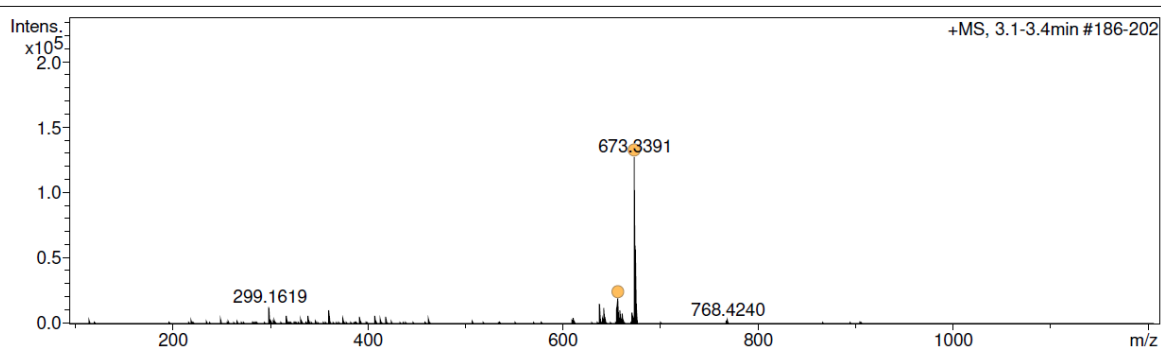


**Figure S16.** HR-ESI-MS spectrum (MeOH) of  $[(L_5^{\text{PhOH}})\text{Fe}^{\text{II}}(\text{MeCN})](\text{PF}_6)_2$ .  $m/z = 656.3001$  (calcd. for  $[(L_5^{\text{PhOH}})\text{Fe}^{\text{II}}(\text{formate})]^+ = 656.3007$ , error = 0.9 ppm),  $m/z = 673.3391$  (calcd. for  $[(L_5^{\text{PhOH}})\text{Fe}^{\text{III}}(\text{OMe})_2]^+ = 673.3398$ , error = 1.0 ppm). NB: sodium formate is used for calibration.

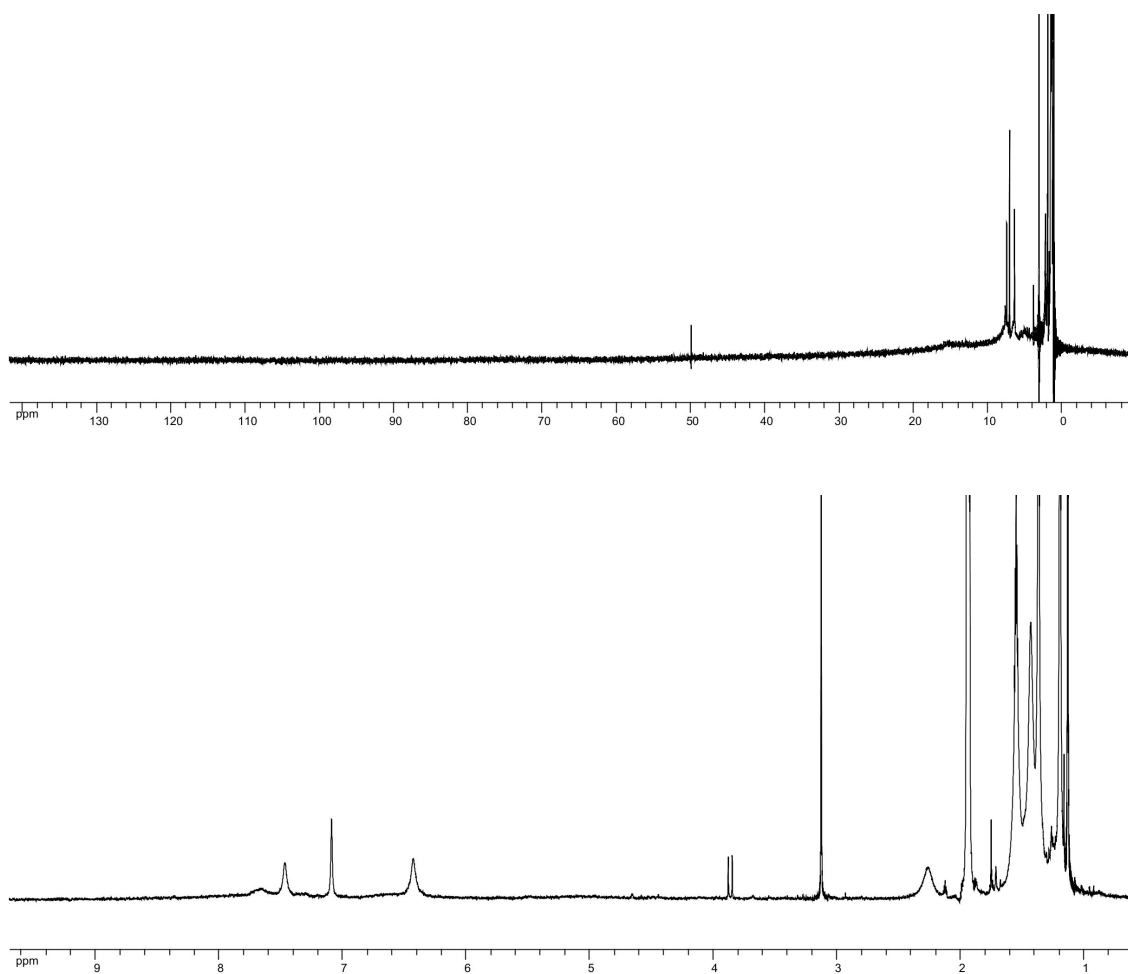


**Figure S17.**  $^1\text{H}$  NMR spectrum ( $\text{CD}_3\text{CN}$ , 360 MHz, 300 K) of  $[(L_5^{\text{PhOH}})\text{Fe}^{\text{II}}(\text{MeCN})](\text{PF}_6)_2$ .

### III.4. $[(L_5^{PhOH})Fe^{II}(OTf)](OTf)$ (**4**)

In a glovebox,  $L_5^{PhOH}$  (138 mg, 0.25 mmol) was suspended in 2 mL MeCN.  $Fe^{II}(OTf)_2$  (87 mg, 0.25 mmol) in 2 mL MeCN were added resulting in a colour change to dark brown. The solution was stirred overnight, filtered. The filtrate was evaporated to dryness to give a sticky oil. It was taken up in tBuOMe and stirred overnight leading to the precipitation of a light tan powder. The product was isolated by filtration (184 mg, 82%)

**UV-vis** (MeCN, 300 K, 0.15 mM). 379 nm ( $\epsilon = 4375 \text{ L}\cdot\text{mol}^{-1}\cdot\text{cm}^{-1}$ ) MLCT  $Fe^{II} \rightarrow py$ ; 315 nm ( $\epsilon = 2400 \text{ L}\cdot\text{mol}^{-1}\cdot\text{cm}^{-1}$ ); 283 nm ( $\epsilon = 3000 \text{ L}\cdot\text{mol}^{-1}\cdot\text{cm}^{-1}$ ); 254 nm ( $\epsilon = 9300 \text{ L}\cdot\text{mol}^{-1}\cdot\text{cm}^{-1}$ )  $\pi-\pi^*$ . The increase in the MLCT extinction coefficient, with respect to **(1)** and **(2)** is indicative of a more pronounced low spin character, in line with the predominant  $[(N_5)Fe^{II}(MeCN)]^{2+}$  species. Furthermore, the spectrum is close to that of **(3)** suggesting a similar binding mode.

**HR-ESI-MS** (MeCN). **C = 0.01 mg/mL**:  $m/z = 656.2982$  (calculated for  $[(L_5^{PhOH})Fe^{II}(HCOO)]^+ = 656.3006$ , error = 6.8 ppm);  $m/z = 673.2915$  (calculated for  $[(L_5^{PhOH})Fe^{III}(HCOO)(OH)]^+ = 673.3028$ , error = 16 ppm). **C = 1 mg/mL**: various fragmentation ions. New peak at  $m/z = 760.2542$  (calculated for  $[(L_5^{PhOH})Fe^{II}(OTf)]^+ = 760.2550$ , error = 1.1 ppm) confirming the presence of the weakly binding triflate, only detectable at higher concentrations.

**CV**. (2 mM in MeCN, WE: GC; CR: Pt; Ref: SCE;  $NBu_4PF_6$  0.1M).  $[(N_5)Fe^{II/III}(MeCN)]^{2+/3+}$  ( $E_p^a = 1.0 \text{ V}$ ,  $E_p^c = 0.89 \text{ V}$ ),  $[(N_5)Fe^{II/III}(OTf)]^{+/2+}$  ( $E_p^a = 0.69 \text{ V}$ ,  $E_p^c = 0.62 \text{ V}$ ) and of the pendant di-tert-butyl-phenol moiety (phenol oxidation at  $E_p^a = 1.61 \text{ V}$ , reduction of the phenolic proton at  $E_p^c = -1.55 \text{ V}$ ).

**Magnetic properties in  $CD_3CN$  solution (Evans method)**.  $[(L_5^{PhOH})Fe^{II}(OTf)](OTf)$  (**4**),  $\mu_{eff} = 3.334 \mu_B$  (64% HS).

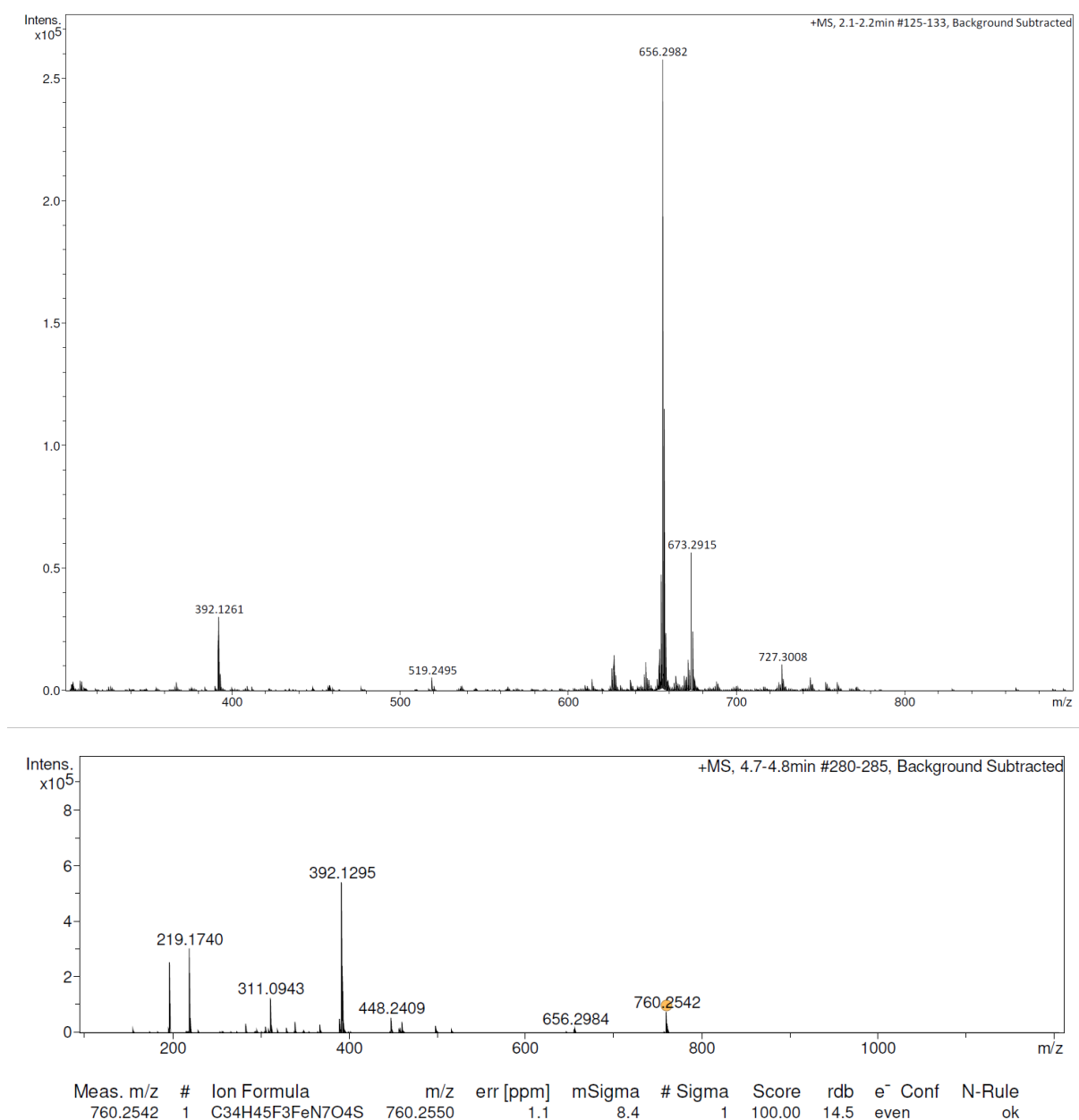


**Figure S18.** HR-ESI-MS spectra (MeCN) of  $[(L_5^{\text{PhOH}})\text{Fe}^{\text{II}}(\text{OTf})](\text{OTf})$  recorded at 0.01 mg/mL (classical MS concentration) and 1 mg/mL (concentrated solution).

**C = 0.01 mg/mL:**  $m/z = 656.2982$  (calculated for  $[(L_5^{\text{PhOH}})\text{Fe}^{\text{II}}(\text{HCOO})]^+ = 656.3006$ , error = 6.8 ppm);  $m/z = 673.2915$  (calculated for  $[(L_5^{\text{PhOH}})\text{Fe}^{\text{III}}(\text{HCOO})(\text{OH})]^+ = 673.3028$ , error = 16 ppm) and unidentified fragmentation ion at  $m/z = 392.1261$  (+1 ion, with an iron containing isotopic pattern)

**C = 1 mg/mL:** various fragmentation ions appear at  $m/z = 219.1740$ ,  $311.0943$ , with an increase in intensity of the  $m/z = 392.1295$  ion. New peak at  $m/z = 760.2542$  (calculated for  $[(L_5^{\text{PhOH}})\text{Fe}^{\text{II}}(\text{OTf})]^+ = 760.2550$ , error = 1.1 ppm) confirming the presence of the weakly binding triflate, only detectable at higher concentrations.

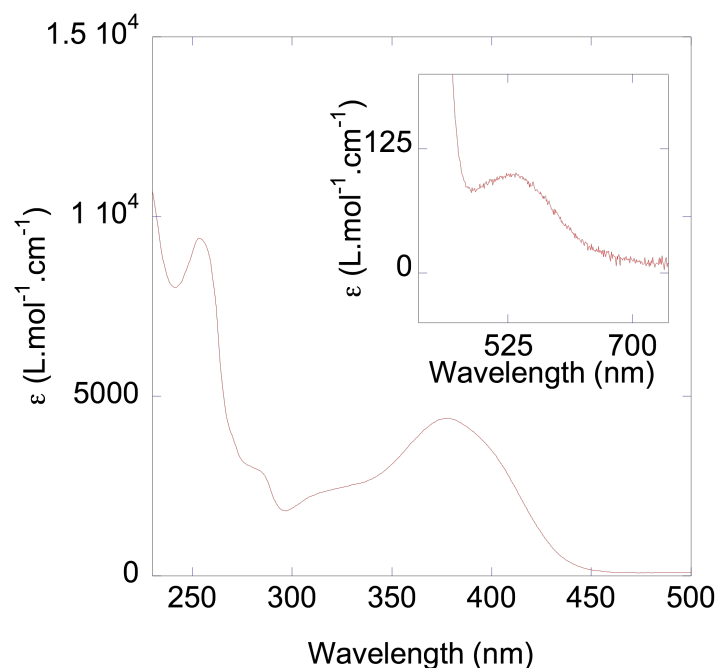


**Figure S19.** UV-vis spectrum of  $[(L_5^{\text{PhOH}})\text{Fe}^{\text{II}}(\text{OTf})](\text{OTf})$  in MeCN, 300 K. 379 nm ( $\epsilon = 4400 \text{ L.mol}^{-1}.\text{cm}^{-1}$ ) MLCT  $\text{Fe}^{\text{II}} \rightarrow \text{py}$ ; 315 nm ( $\epsilon = 2300 \text{ L.mol}^{-1}.\text{cm}^{-1}$ ); 283 nm ( $\epsilon = 3000 \text{ L.mol}^{-1}.\text{cm}^{-1}$ ); 254 nm ( $\epsilon = 9300 \text{ L.mol}^{-1}.\text{cm}^{-1}$ )  $\pi-\pi^*$

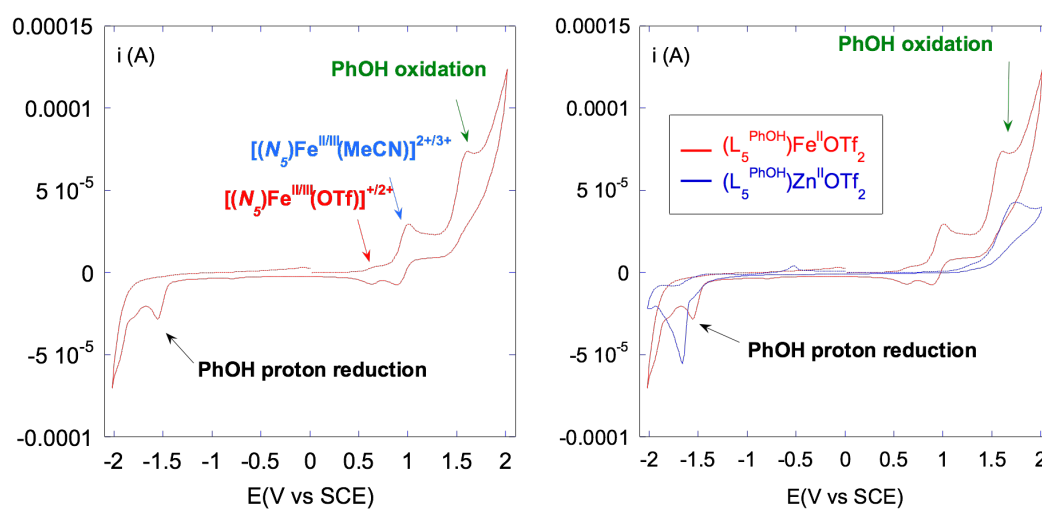


**Figure S20.** CV of  $[(L_5^{\text{PhOH}})\text{Fe}^{\text{II}}(\text{OTf})](\text{OTf})$  (left, 2 mM in MeCN,  $\text{NBu}_4\text{PF}_6$  0.1M).

The CV displays the signatures of the couples  $[(N_5)\text{Fe}^{\text{II/III}}(\text{MeCN})]^{2+/3+}$  ( $E_p^a = 1.0 \text{ V}$ ,  $E_p^c = 0.89 \text{ V}$ ),  $[(N_5)\text{Fe}^{\text{II/III}}(\text{OTf})]^{+/2+}$  ( $E_p^a = 0.69 \text{ V}$ ,  $E_p^c = 0.62 \text{ V}$ ) and of the pendant di-tert-butyl-phenol moiety (phenol oxidation at  $E_p^a = 1.61 \text{ V}$ , and reduction of the phenolic proton at  $E_p^c = -1.55 \text{ V}$ . Overlay of the CVs of  $[(L_5^{\text{PhOH}})\text{Fe}^{\text{II}}(\text{OTf})](\text{OTf})$  and  $[(L_5^{\text{PhOH}})\text{Zn}^{\text{II}}(\text{OTf})](\text{OTf})$  (right).

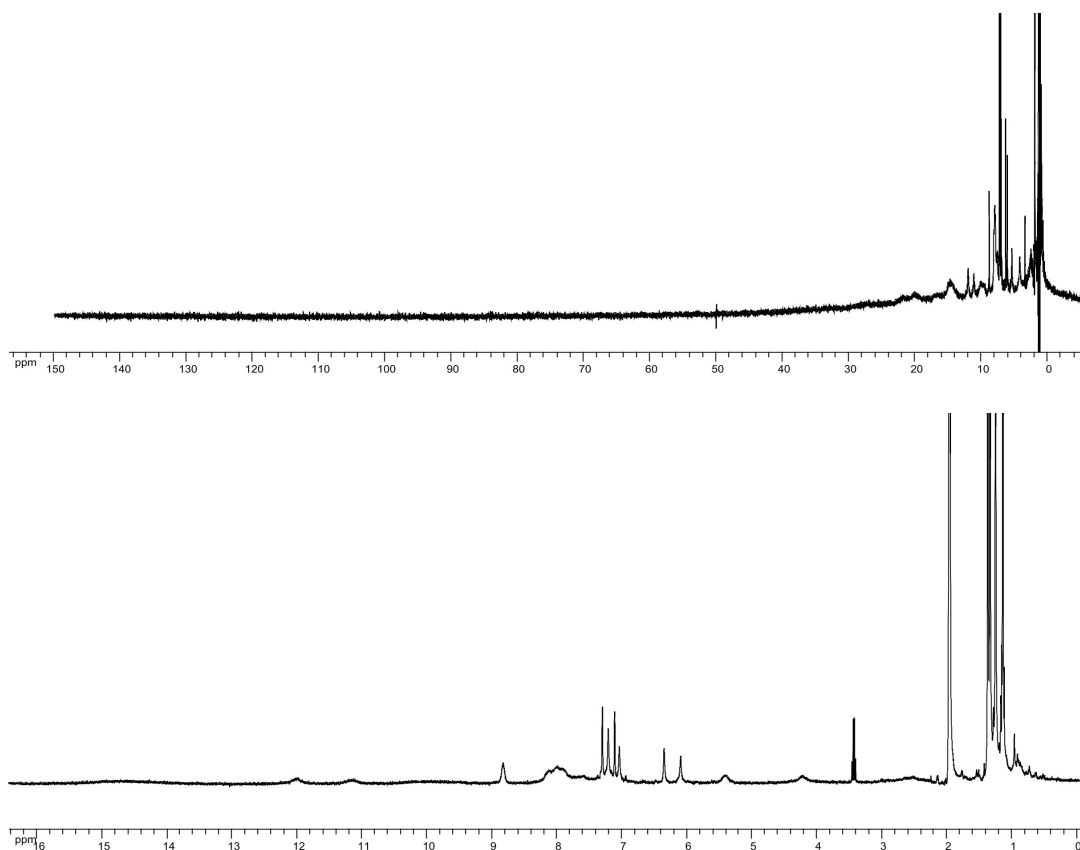


**Figure S21.**  $^1\text{H}$  NMR spectrum ( $\text{CD}_3\text{CN}$ , 360 MHz, 300 K) of  $[(\text{L}_5^{\text{PhOH}})\text{Fe}^{\text{II}}(\text{OTf})](\text{OTf})$ .

### ***III.5. Determination of the magnetic moment of the complexes by the Evans NMR method.<sup>[9]</sup>***

Coaxial NMR tubes were used.

The inner capillary tube contains a solution of TMS in  $\text{CD}_3\text{CN}$  ( $1\mu\text{L}$  in  $1\text{mL}$   $\text{CD}_3\text{CN}$ ). The outer tube contains the complex ( $m = 10\text{ mg/mL}$ ) with  $1\mu\text{L}$  of TMS for  $1\text{mL}$   $\text{CD}_3\text{CN}$ . The paramagnetic shift was measured on TMS and on the residual  $\text{CD}_3\text{CN}$  peak and gave similar values.

The general formula for the mass susceptibility is:

$$\chi_g = -3\Delta f / (4\pi F m) + [\chi^\circ + \chi^\circ(d^\circ - d^s) / m]$$

Where  $m$  is the mass of complex (in g) in 1 mL of solution,  $\Delta f$  is the separation between the peaks (TMS or  $\text{CD}_3\text{CN}$ ) of the inner and outer tubes in Hz,  $F$  is the frequency of the spectrometer in Hz (360 MHz here),  $\chi^\circ$  is the susceptibility of the pure solvent,  $d^\circ$  the density of the solvent,  $d^s$  the density of the complex solution.

In the present case, with dilute solutions (around 11 mM),  $d^s$  can be approximated to  $(d^\circ + m)$  and the expression simplifies to:

$$\chi_g = -3\Delta f / (4\pi F m)$$

The molar susceptibility is  $\chi_M = M \times \chi_g$  and the paramagnetic susceptibility is given by  $\chi_{\text{para}} = \chi_M - \chi_{\text{dia}}$ .

The diamagnetic corrections  $\chi_{\text{dia}}$  were determined using Pascal's constants.<sup>[10]</sup>

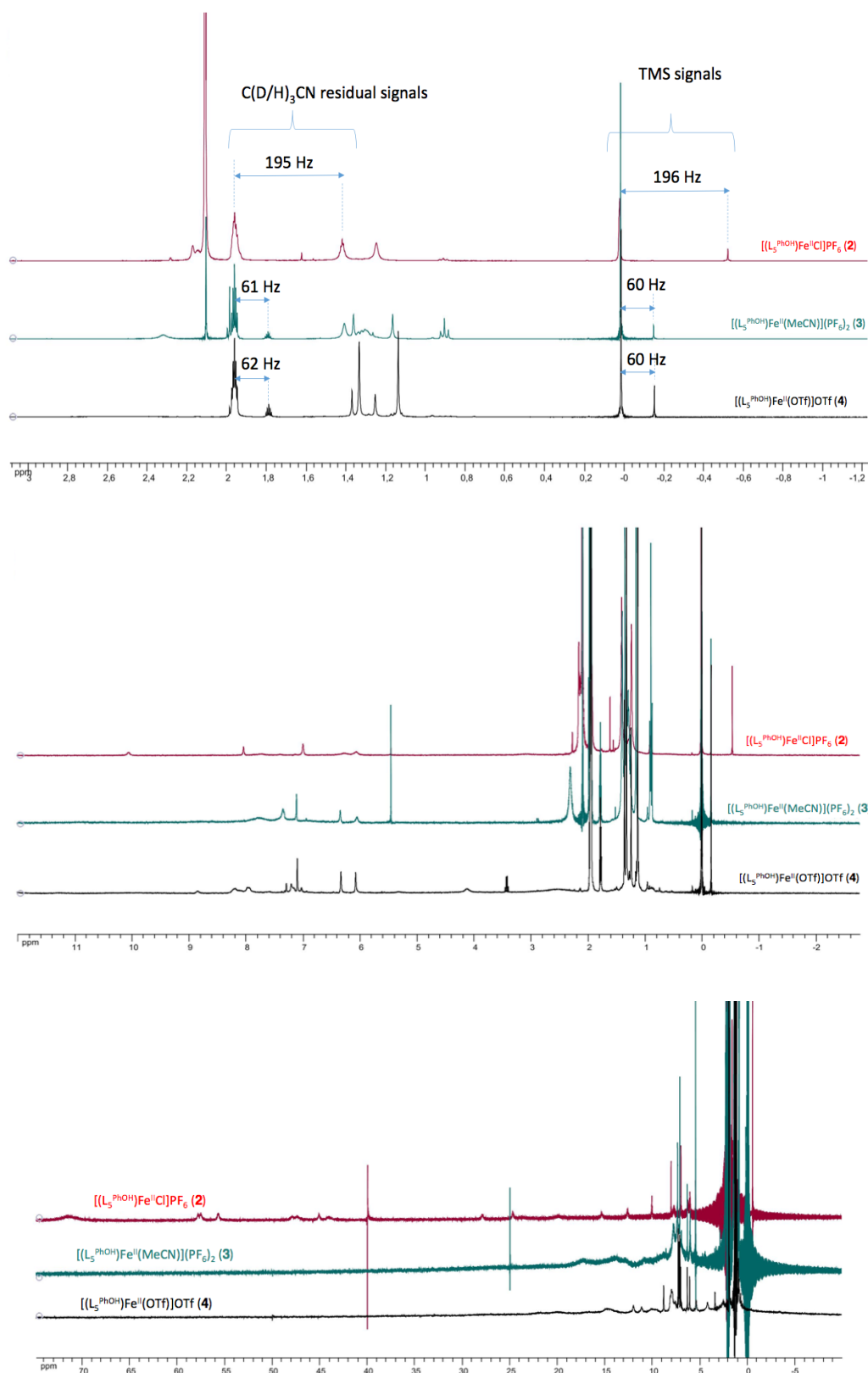


**Figure S22.**  $^1\text{H}$  NMR spectra ( $\text{CD}_3\text{CN}$ , 360 MHz, 300 K) of  $[(\text{L}_5^{\text{PhOH}})\text{Fe}^{\text{II}}\text{Cl}]\text{PF}_6$  (2),  $[(\text{L}_5^{\text{PhOH}})\text{Fe}^{\text{II}}(\text{MeCN})](\text{PF}_6)_2$  (3), and  $[(\text{L}_5^{\text{PhOH}})\text{Fe}^{\text{II}}(\text{OTf})](\text{OTf})$  (4), in the presence of TMS as an internal standard, in the coaxial tubes setup of Evans Method.

For the 3 complexes,  $m = 10^{-2}$  g/mL,  $F = 360 \times 10^6$  Hz

For  $[(L_5^{PhOH})Fe^{II}Cl]PF_6$  (**2**),  $\Delta f = 195$  Hz,  $M = 791$  g.mol $^{-1}$ ,  $\chi_{dia} = -434.10^{-6}$  emu.mol $^{-1}$  and thus  $\chi_{para} = 0.00425097$  emu.mol $^{-1}$

For  $[(L_5^{PhOH})Fe^{II}(MeCN)](PF_6)_2$  (**3**),  $\Delta f = 60$  Hz,  $M = 942$  g.mol $^{-1}$ ,  $\chi_{dia} = -502.10^{-6}$  emu.mol $^{-1}$  and thus  $\chi_{para} = -0.01066565$  emu.mol $^{-1}$

For  $[(L_5^{PhOH})Fe^{II}(OTf)](OTf)$  (**4**),  $\Delta f = 60$  Hz,  $M = 909$  g.mol $^{-1}$ ,  $\chi_{dia} = -448.10^{-6}$  emu.mol $^{-1}$  and thus  $\chi_{para} = -0.000463454$  emu.mol $^{-1}$ .

$$\mu_{eff} = 2.828\sqrt{\chi_{para}T}$$

For a high spin  $S=2$   $Fe^{II}$  complex, with  $g = 2.1$   $\mu_{eff} = g\mu_B\sqrt{S(S+1)} = 5.1439$

Considering an equilibrium between HS  $S=2$  and LS  $S=0$  species:

For  $[(L_5^{PhOH})Fe^{II}Cl]PF_6$  (**2**),  $\mu_{eff} = 5.058 \mu_B$  (98% HS).

For  $[(L_5^{PhOH})Fe^{II}(MeCN)](PF_6)_2$  (**3**),  $\mu_{eff} = 3.193 \mu_B$  (62% HS).

For  $[(L_5^{PhOH})Fe^{II}(OTf)](OTf)$  (**4**),  $\mu_{eff} = 3.334 \mu_B$  (64% HS).

This confirms that complex (**4**) displays the same magnetic behaviour as (**3**) in MeCN, owing to a similar first coordination sphere. The difference in resonances observed by NMR are ascribed to the coordination kinetic exchange OTf/MeCN in the case of (**4**) that is prevented in the case of (**3**).

It also confirms the UV-vis interpretation, based on the extinction coefficients, that (**2**) displays a much larger paramagnetic contribution to the spin equilibrium than (**4**).

## IV/ Reactivity studies

### IV.1. Reaction of $[(L_5^{PhOH})Fe^{II}(OTf)](OTf)$ (4) with PhIO.

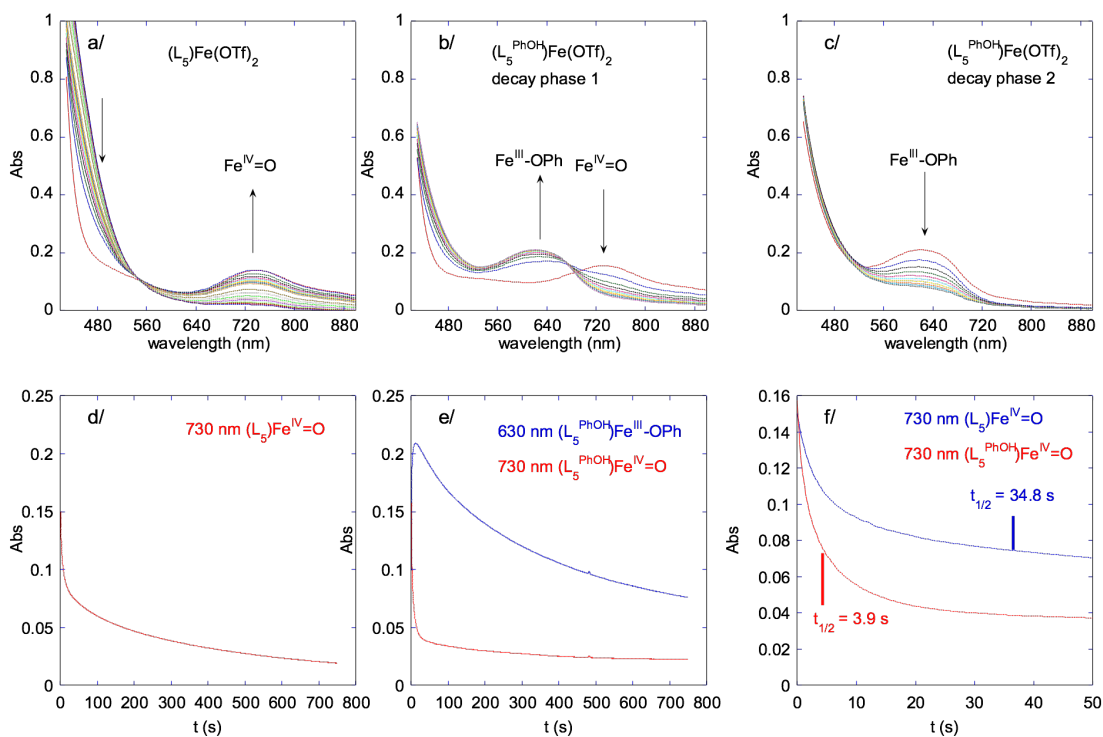


**Figure S23.** Evolution of the UV-vis spectrum during the decay of the  $Fe^{IV}O$  species generated by mixing a 1 mM solution of  $[(L_5)Fe^{II}(OTf)](OTf)$  (a/) or  $[(L_5^{PhOH})Fe^{II}(OTf)](OTf)$  (b/ and c/) in MeCN with 1.2 equiv. PhIO at 293 K. Timetraces at 730 nm for  $[(L_5)Fe^{IV}O]^{2+}$  decay (d/) and at 730 and 630 nm for  $[(L_5^{PhOH})Fe^{IV}O]^{2+}$  decay and  $[(L_5^{PhOH})Fe^{III}(OPh)]^{2+}$  growth and decay (e/). Comparison of the timetraces at 730 nm for  $[(L_5)Fe^{IV}O]^{2+}$  and  $[(L_5^{PhOH})Fe^{IV}O]^{2+}$  decay and corresponding  $t_{1/2}$  values of the  $Fe^{IV}O$  species.

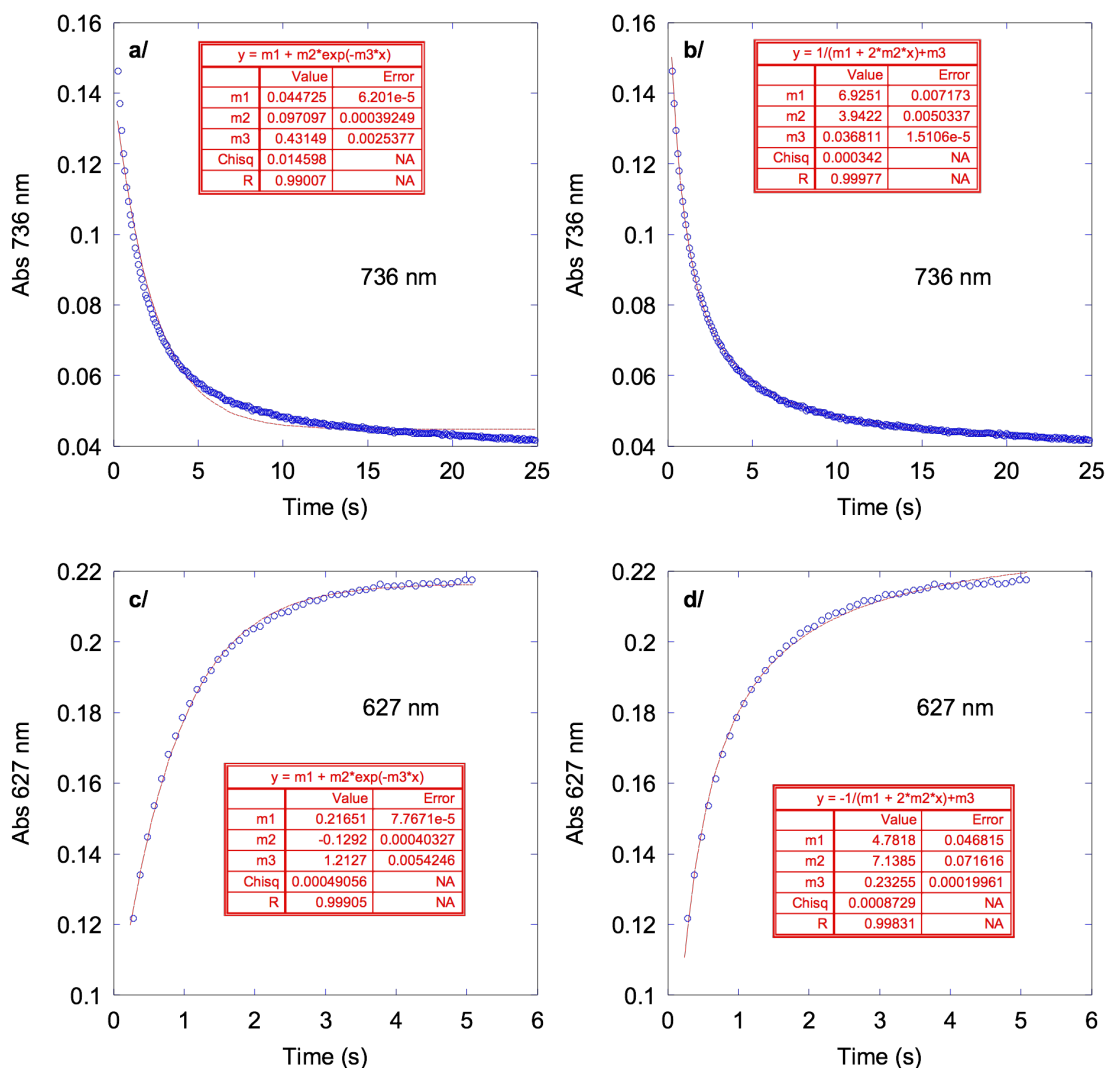


**Figure S24.** Experimental timetraces at 736 nm (a/ and b/, blue circles) recorded during the decay of the  $\text{Fe}^{\text{IV}}\text{O}$  species and at 627 nm (c/ and d/, blue circles) during the growth of the  $\text{Fe}^{\text{III}}(\text{OPh})$  species after mixing a 1 mM solution of  $[(\text{L}_5^{\text{PhOH}})\text{Fe}^{\text{II}}(\text{OTf})](\text{OTf})$  in MeCN with 1.2 equiv. PhIO at 293 K and simulated timetraces (red lines) obtained by fitting the data to a monoexponential law (a/ and c/) and a 2<sup>nd</sup> order law (b/ and d/).

**Comment :** The decay of  $\text{Fe}^{\text{IV}}\text{O}$  is best described by a bimolecular mechanism ( $k_2 = 2m2 = 7.8 \text{ L} \cdot \text{mol}^{-1} \cdot \text{s}^{-1}$ ). In contrast, the growth of the  $\text{Fe}^{\text{III}}(\text{OPh})$  can be described by a first or second order law in the same way most likely because this step is not an elementary one, as described in Scheme 1, main text.

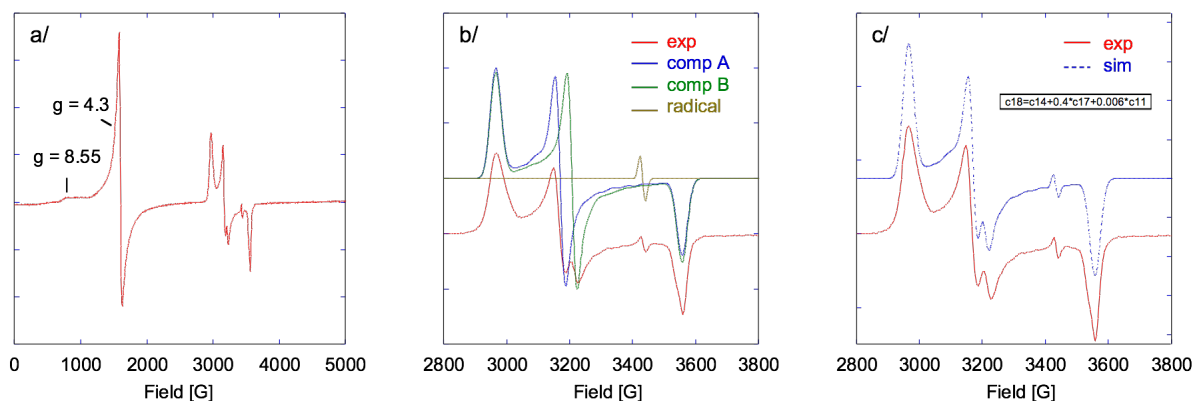


**Figure S25.** X band EPR spectrum in MeCN (90 K) of the ~~green~~ solution obtained just after the addition of 1.2 equiv. PhIO (in MeCN/MeOH) to a 2 mM solution of  $[(L_5^{PhOH})Fe^{II}(OTf)](OTf)$  in MeCN at room temperature (a/). Experimental spectrum and different simulated spectra of the components of the LS signal (b/). Experimental spectrum and summed simulated spectrum of the 3 components. *Component A*:  $g = 2.32 \ 2.17 \ 1.935$ ; *Component B*:  $g = 2.32 \ 2.145 \ 1.935$ ; *radical*:  $g = 2.004$ . A and B are ascribed to two different  $Fe^{III}(OMe)$  species likely corresponding to  $(N_5)Fe^{III}(OMe)^{2+}$  and  $(N_4)Fe^{III}(OMe)(MeCN)^{2+}$ . Relative weight of the two LS iron components in the simulation:  $A / B = 1 / 0.4$ .

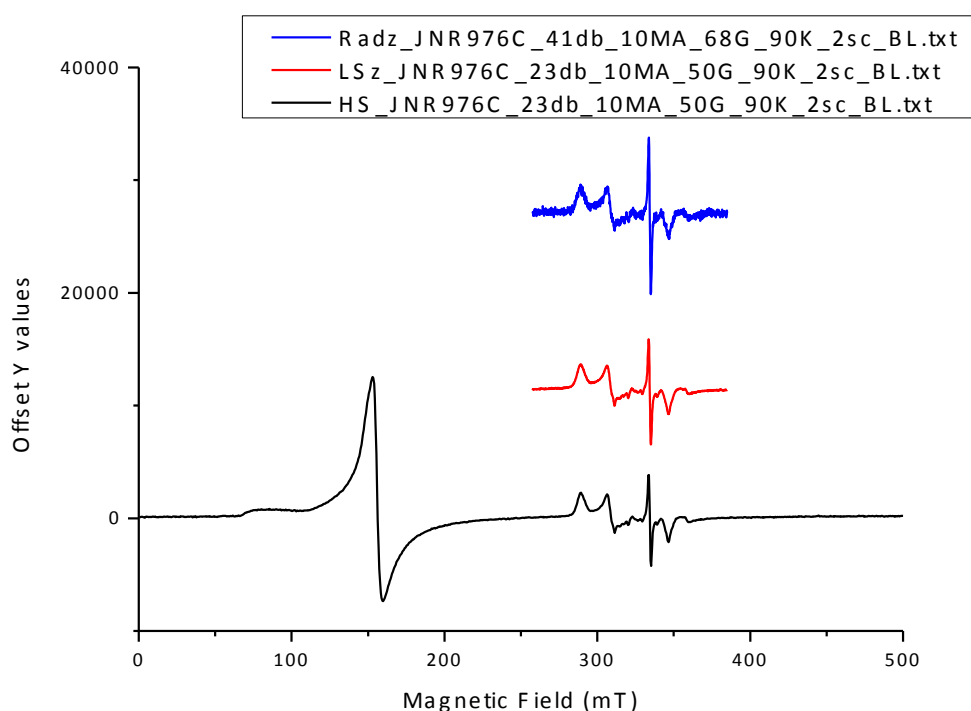


**Figure S26.** X band EPR spectra in MeCN (90 K) of the solution obtained after the addition of 1.2 equiv. PhIO (in MeCN/MeOH, at RT) to a 2 mM solution of  $[(L_5^{PhOH})Fe^{II}(OTf)](OTf)$  (in MeCN at  $-40^\circ C$ . Estimated temperature after mixing:  $-10^\circ C$ ) followed by immediate freezing in liquid nitrogen. Recorded at 23 dB attenuation (suited for iron species) and 41 dB attenuation (suited for radical species).  $[Fe] = 2mM$ . The spectrum displays a HS species at  $g = 4.3$  ( $Fe^{III}-OPh$ ), a low spin  $Fe^{III}$  signal ( $g = 2.318 \ 2.170 \ 1.943$ ) and a radical species. They were quantified against  $Fe^{III}(EDTA)^-$ ,  $Cu(SO_4)$  and TEMPO standards respectively).  $[HS \ Fe^{III}] = 0.46 \ mM$ ,  $[LS \ Fe^{III}] = 0.10 \ mM$ ,  $[radical] = 0.02 \ mM$ .

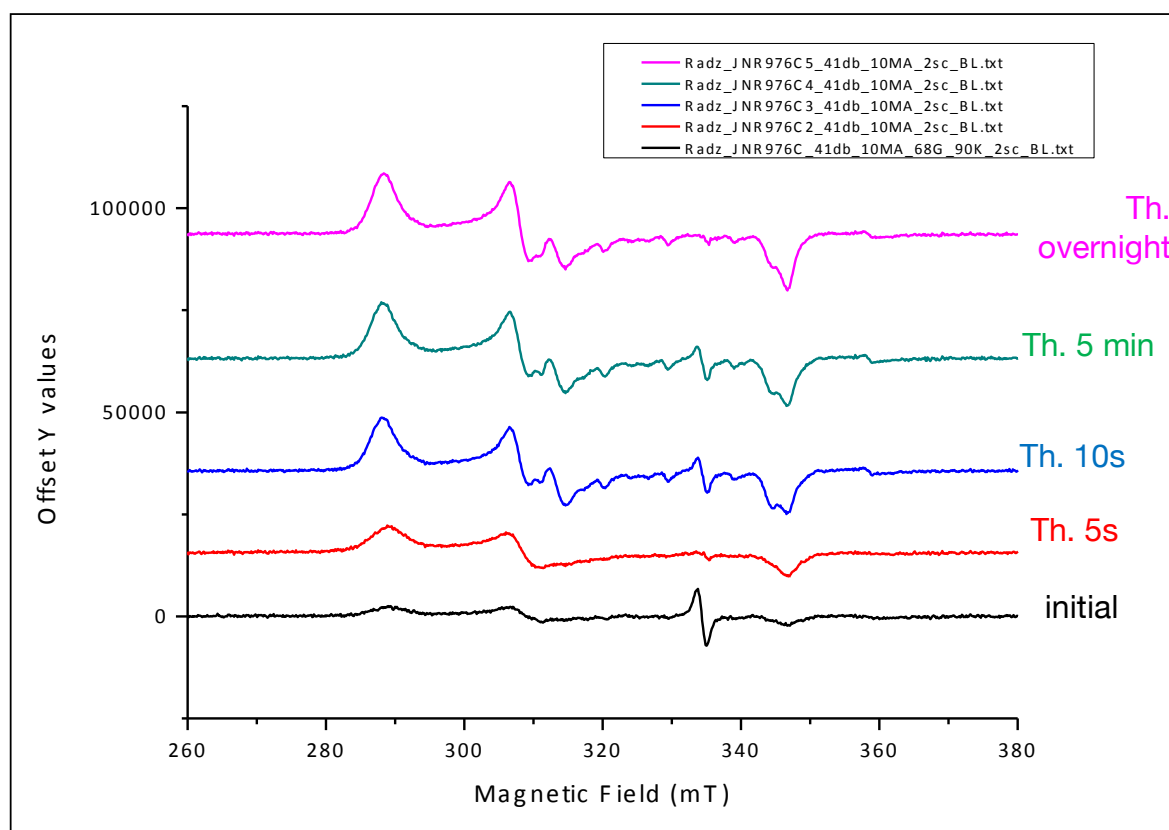
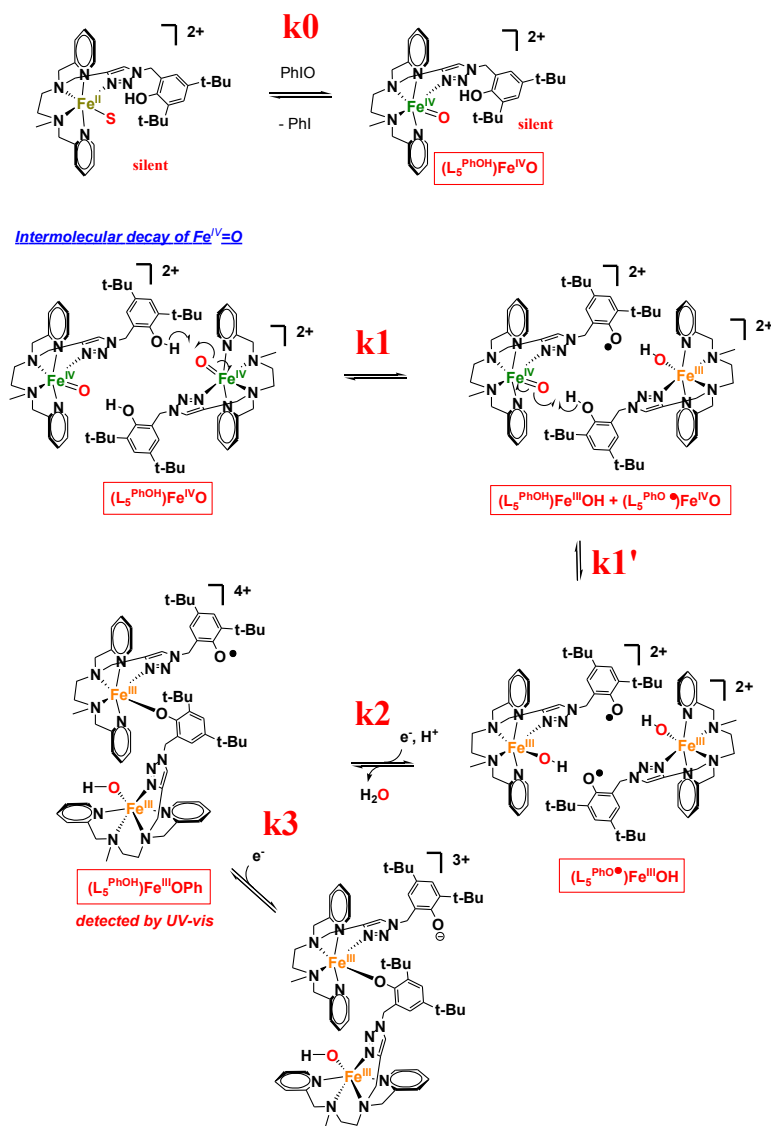


**Figure S27.** Evolution upon thawing the tube to RT of the X band EPR spectra in MeCN (90 K) of the solution obtained after the addition of 1.2 equiv. PhIO (in MeCN/MeOH, at RT) to a 2 mM solution of  $[(L_5^{PhOH})Fe^{II}(OTf)](OTf)$  (in MeCN at  $-40^\circ\text{C}$ . Estimated temperature after mixing:  $-10^\circ\text{C}$ ) followed by immediate freezing in liquid nitrogen. In a 1<sup>st</sup> step, the radical vanishes (5s). In a 2<sup>nd</sup> step, it reappears alongside a next LS  $Fe^{III}$  species (10 s, 5 min), and in a last step, the radical vanishes again over hours.



**Scheme S4.** Proposed mechanism for the evolution of the Fe<sup>IV</sup>O and phenoxyl radical species. The electron used for the reduction can either come from Fe<sup>II</sup> or from an organic substrate (methanol or ligand)

**Comment:** Right after mixing, i) the predominant species is the HS Fe<sup>III</sup> one, which indicates that the overall reaction (from Fe<sup>II</sup> to Fe<sup>III</sup>-OPh) is very fast, and ii) the LS Fe<sup>III</sup>/radical ratio is way above 1. In the mechanism we proposed (Scheme S4), Fe<sup>II</sup> reacts with PhIO to yield Fe<sup>IV</sup>O.

Both Fe<sup>II</sup> and Fe<sup>IV</sup>O are EPR-silent (k<sub>0</sub>). Then, an intermolecular reaction occurs where Fe<sup>IV</sup>O reacts with the phenol to yield Fe<sup>III</sup>-OH and the radical (steps k<sub>1</sub> and k<sub>1</sub>'). At this stage, a 1:1 ratio between the two species is expected. The following step is the reduction of the radical by a scavenger in the reaction medium (remaining Fe<sup>II</sup>, methanol or an oxidizable site of the ligand) and the generation of the Fe<sup>III</sup>-OPh moiety (k<sub>2</sub>, k<sub>3</sub> steps, HS signal g = 4.3 in EPR). If k<sub>2</sub>, k<sub>3</sub> are fast compared to k<sub>1</sub>, k<sub>1</sub>' (which is likely, given that the HS signal is predominant right from the start), the amount of radical will be much smaller than that of the LS Fe<sup>III</sup> species. The process is supported by the evolution upon 5s thawing: the radical vanishes. Interestingly, when the thawing process was repeated, the overall LS Fe<sup>III</sup> keeps on increasing, a new set of LS Fe<sup>III</sup> signal appears (g = 2.332 2.137 1.944) and a trace amount of radical re-appears. The latter remains visible over 5 min and disappears overnight.

The new set of LS Fe<sup>III</sup> signal can be ascribed to the decoordination of triazole and formation of a [(N<sub>4</sub>)Fe<sup>III</sup>(MeCN)(OMe)]<sup>2+</sup> species. Such decoordination was observed in the Fe<sup>III</sup>OOH species of the parent L<sub>5</sub> complex deprived of phenol.<sup>[11]</sup> The reappearance of the radical indicates that the initial radical scavenger is likely to be the remaining Fe<sup>II</sup>, which reacts quickly with the radical. Indeed, it can be seen on the UV-vis timetraces (Figure 2c) that the Fe<sup>III</sup>Oph chromophore (637 nm) already appears before the Fe<sup>IV</sup>O chromophore (730 nm) reaches its apex. So the transient radical will be exposed to remaining Fe<sup>II</sup> in solution. As long as Fe<sup>II</sup> is present, it will scavenge the radical, hence its initial disappearance. Once Fe<sup>II</sup> is depleted, the residual radical is more persistent and can be detected over a few minutes. It vanishes overnight by slower reactions, with either the solvent or by oxidizing weak sites of the ligand.

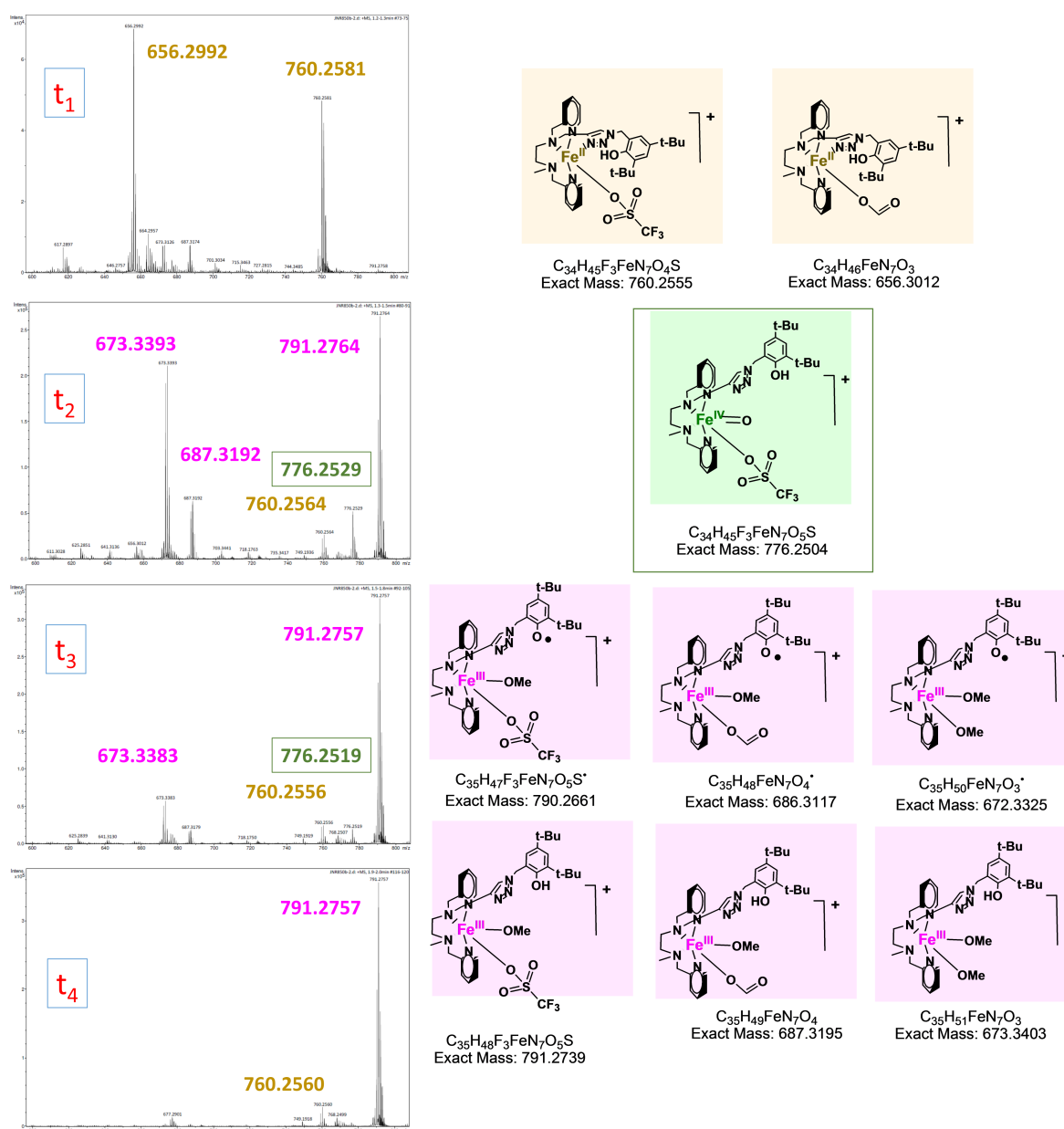


**Figure S28.** Time evolution of the mass spectrum of a solution injected immediately after mixing [(L<sub>5</sub><sup>PhOH</sup>)Fe<sup>II</sup>(OTf)](OTf) in MeCN with 1.2 equiv. PhIO at 293 K. The sample was continuously injected

and the spectra continually recorded. The timeframes correspond to the following intervals:  $t_1 = [0.0 \text{ min}-0.1 \text{ min}]$ ;  $t_2 = [0.1 \text{ min}-0.3 \text{ min}]$ ;  $t_3 = [0.3 \text{ min}-0.6 \text{ min}]$ ;  $t_4 = [0.7 \text{ min}-0.8 \text{ min}]$ .

**Comment :** The initial  $\text{Fe}^{\text{II}}$  complex ( $m/z = 656.3$  and  $760.2$ ) disappears concomitantly with the formation of a transient  $\text{Fe}^{\text{IV}}\text{O}$  species ( $m/z = 776.2$ ) which evolves towards the final  $\text{Fe}^{\text{III}}$  species (peaks at  $m/z = 673.3$ ,  $687.3$  and  $791.2$ ).

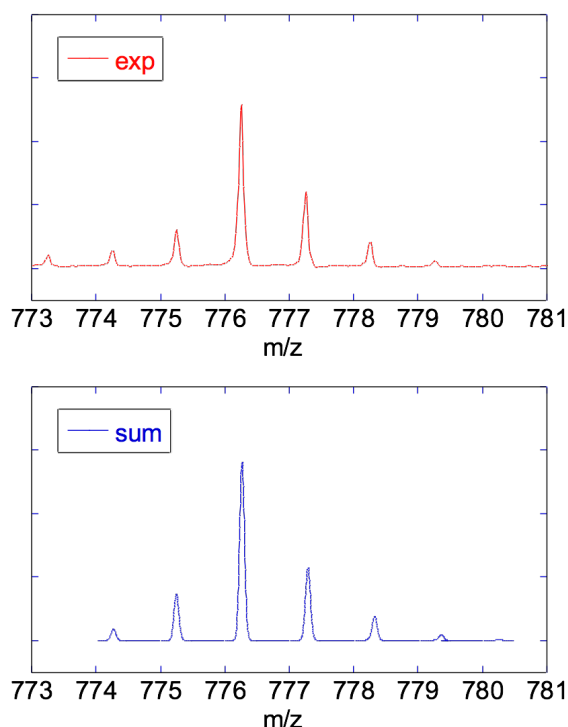
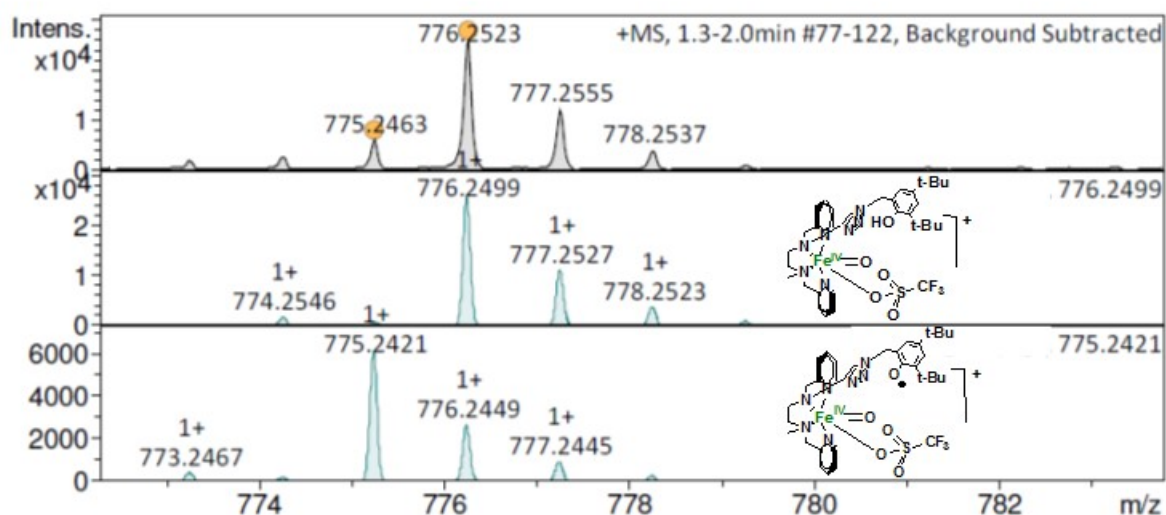


**Figure S29.** Upper part: Experimental (top) vs individual simulated mass spectra (middle, bottom) showing the pattern of the  $\text{Fe}^{\text{IV}}\text{O}$  species ( $m/z = 775/776$ ), detected upon mixing  $[(\text{L}_5^{\text{PhOH}})\text{Fe}^{\text{II}}(\text{OTf})](\text{OTf})$  in MeCN with 1.2 equiv. PhIO at 293 K.  $m/z$  calcd for  $[(\text{L}_5^{\text{PhOH}})\text{Fe}^{\text{IV}}(\text{O})(\text{OTf})]^+$ : 776.2499, error = 3.1 ppm),  $m/z$  calcd for  $[(\text{L}_5^{\text{PhOH}})\text{Fe}^{\text{IV}}(\text{O})(\text{OTf})]^+$ : 775.2421, error = 5.4 ppm). Lower

part: experimental spectrum vs weighted sum of the two simulated contributions  $[(L_5^{\text{PhOH}})\text{Fe}^{\text{IV}}(\text{O})(\text{OTf})]^+$  and  $[(L_5^{\text{PhO}^{\bullet}})\text{Fe}^{\text{IV}}(\text{O})(\text{OTf})]^+$ .

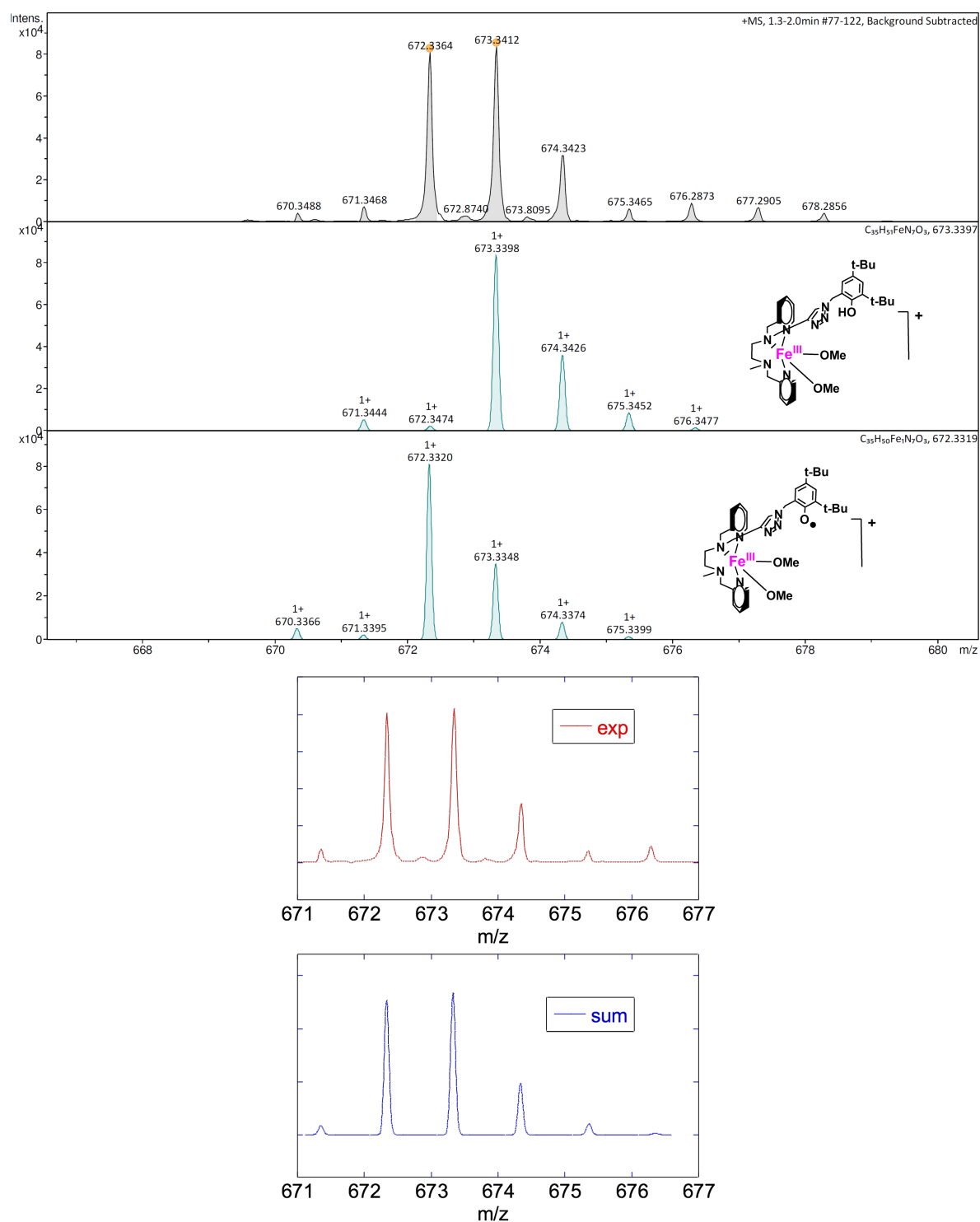


**Figure S30.** Upper part: Experimental (top) vs individual simulated mass spectra (middle, bottom) showing the pattern of the  $\text{Fe}^{\text{III}}(\text{OMe})_2$  species ( $m/z = 672/673$ ), detected upon mixing  $[(L_5^{\text{PhOH}})\text{Fe}^{\text{II}}(\text{OTf})](\text{OTf})$  in MeCN with 1.2 equiv. PhIO at 293 K.  $m/z$  calcd for  $[(L_5^{\text{PhOH}})\text{Fe}^{\text{III}}(\text{OMe})_2]^+$ : 673.3397, error = 2.1 ppm),  $m/z$  calcd for  $[(L_5^{\text{PhO}^{\bullet}})\text{Fe}^{\text{III}}(\text{OMe})_2]^+$ : 672.3319, error = 6.5 ppm). Lower part: weighted sum of the two simulated contributions  $[(L_5^{\text{PhOH}})\text{Fe}^{\text{III}}(\text{OMe})_2]^+$  and  $[(L_5^{\text{PhO}^{\bullet}})\text{Fe}^{\text{III}}(\text{OMe})_2]^+$ .

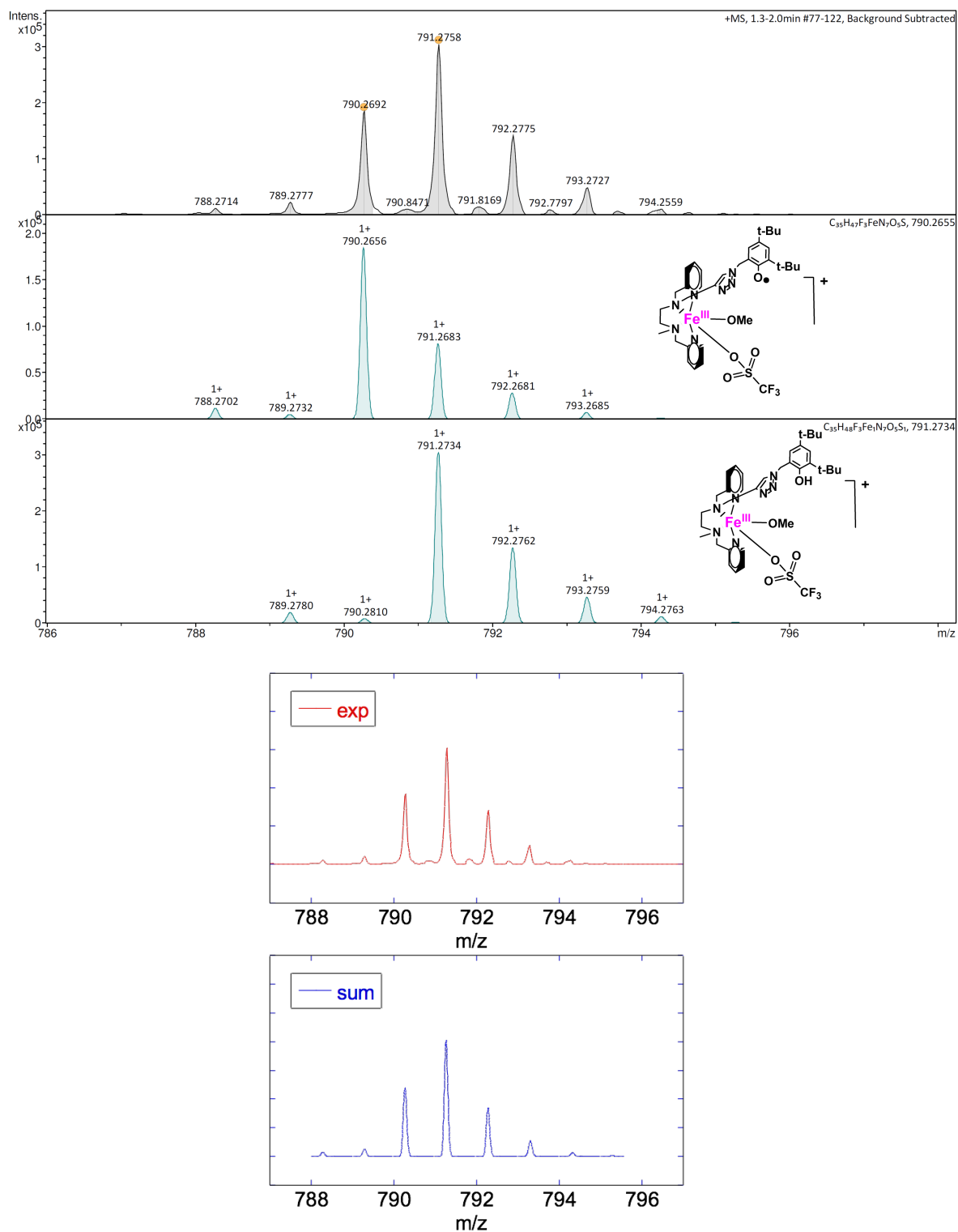


**Figure S31.** Upper part: Experimental (top) vs individual simulated mass spectra (middle, bottom) showing the pattern of the  $\text{Fe}^{\text{III}}(\text{OMe})(\text{OTf})$  species ( $m/z = 790/791$ ), detected upon mixing  $[(\text{L}_5^{\text{PhOH}})\text{Fe}^{\text{II}}(\text{OTf})](\text{OTf})$  in MeCN with 1.2 equiv. PhIO at 293 K.  $m/z$  calcd for  $[(\text{L}_5^{\text{PhOH}})\text{Fe}^{\text{III}}(\text{OMe})(\text{OTf})]^+$ : 791.2734, error = 3.1 ppm,  $m/z$  calcd for  $[(\text{L}_5^{\text{PhO}^*})\text{Fe}^{\text{III}}(\text{OMe})(\text{OTf})]^+$ : 790.2655, error = 4.5 ppm. Lower part: weighted sum of the two simulated contributions  $[(\text{L}_5^{\text{PhOH}})\text{Fe}^{\text{III}}(\text{OMe})(\text{OTf})]^+$  and  $[(\text{L}_5^{\text{PhO}^*})\text{Fe}^{\text{III}}(\text{OMe})(\text{OTf})]^+$ .

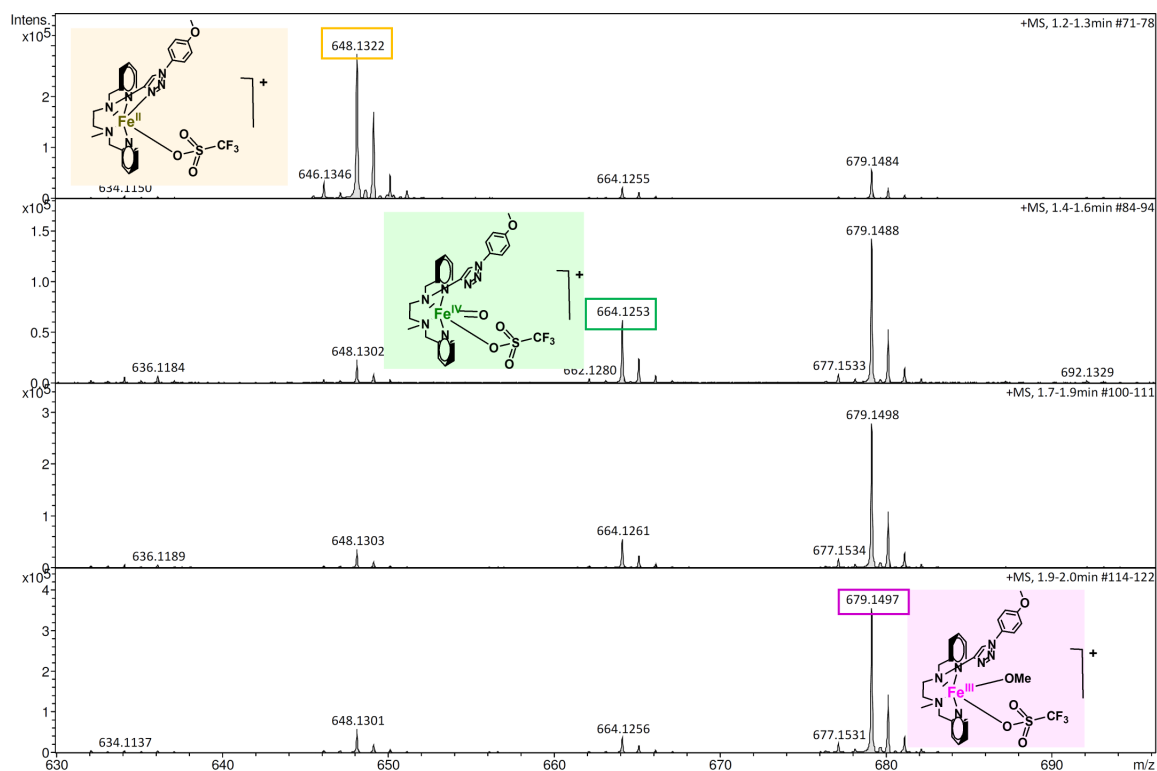


**Figure S32.** Time evolution of the mass spectrum of a solution injected immediately after mixing  $[(L_5)Fe^{II}(OTf)](OTf)$  in MeCN with 1.2 equiv. PhIO at 293 K.

**Comment :** The initial  $Fe^{II}$  complex ( $m/z = 648.1$ ) disappears in favor of a transient  $Fe^{IV}O$  species ( $m/z = 664.1$ ) which evolves towards the final  $Fe^{III}$  species ( $m/z = 679.1$ ).

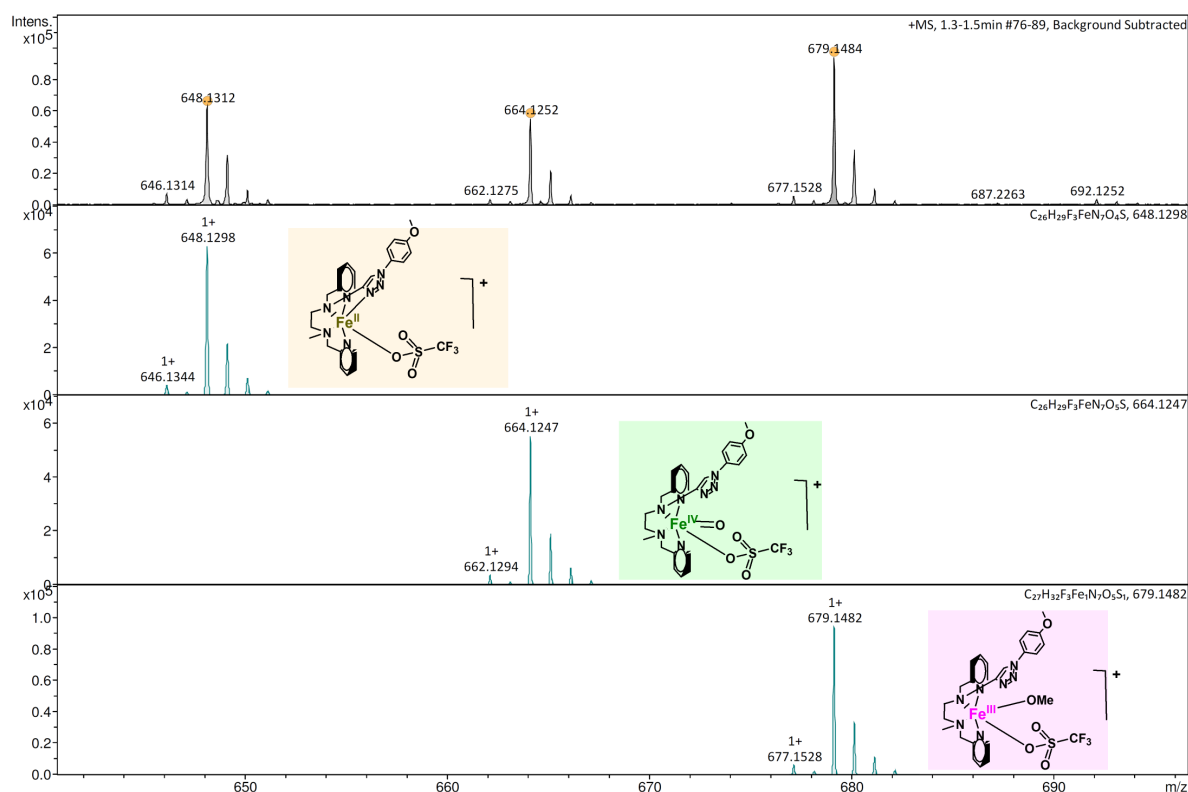


**Figure S33.** Experimental (top) vs simulated mass spectra showing the pattern of the Fe<sup>II</sup> ( $m/z = 648.13$ ), Fe<sup>IV</sup>O ( $m/z = 664.12$ ) and Fe<sup>III</sup> ( $m/z = 679.14$ ) species detected upon mixing **[(L<sub>5</sub>)Fe<sup>II</sup>(OTf)](OTf)** in MeCN with 1.2 equiv. PhIO at 293 K.  $m/z = 648.1312$  (calcd for **[(L<sub>5</sub>)Fe<sup>II</sup>(OTf)]<sup>+</sup>**: 648.1298, error = 2 ppm),  $m/z = 664.1252$  (calcd for **[(L<sub>5</sub>)Fe<sup>IV</sup>(O)(OTf)]<sup>+</sup>**: 664.1247, error = 0.7 ppm),  $m/z = 679.1484$  (calcd for **[(L<sub>5</sub>)Fe(OMe)(OTf)]<sup>+</sup>**: 679.1482, error = 0.3 ppm).

**Table S1.** Oxidation of cyclooctene by iodobenzene catalyzed by **[(L<sub>5</sub><sup>PhOH</sup>)Fe<sup>II</sup>(OTf)](OTf)** and **[(L<sub>5</sub>)Fe<sup>II</sup>(OTf)](OTf)** at room temperature.<sup>[a]</sup> % Yields are given with respect to the oxidant.

Substrate			cyclooctene <sup>[a]</sup>	
Products			epox	diol
entry	Oxidant	Catalyst		
1	PhIO	<b>[(L<sub>5</sub><sup>PhOH</sup>)Fe<sup>II</sup>(OTf)](OTf)</b>	15.5	3.5
2	PhIO	<b>[(L<sub>5</sub>)Fe<sup>II</sup>(OTf)](OTf)</b>	21.2	3

<sup>[a]</sup> Fe / PhIO / cyclooctene : 1 / 2 / 800. Cyclooctene oxide and cyclooctane-1,2-diol are denoted epoxide and diol, respectively.

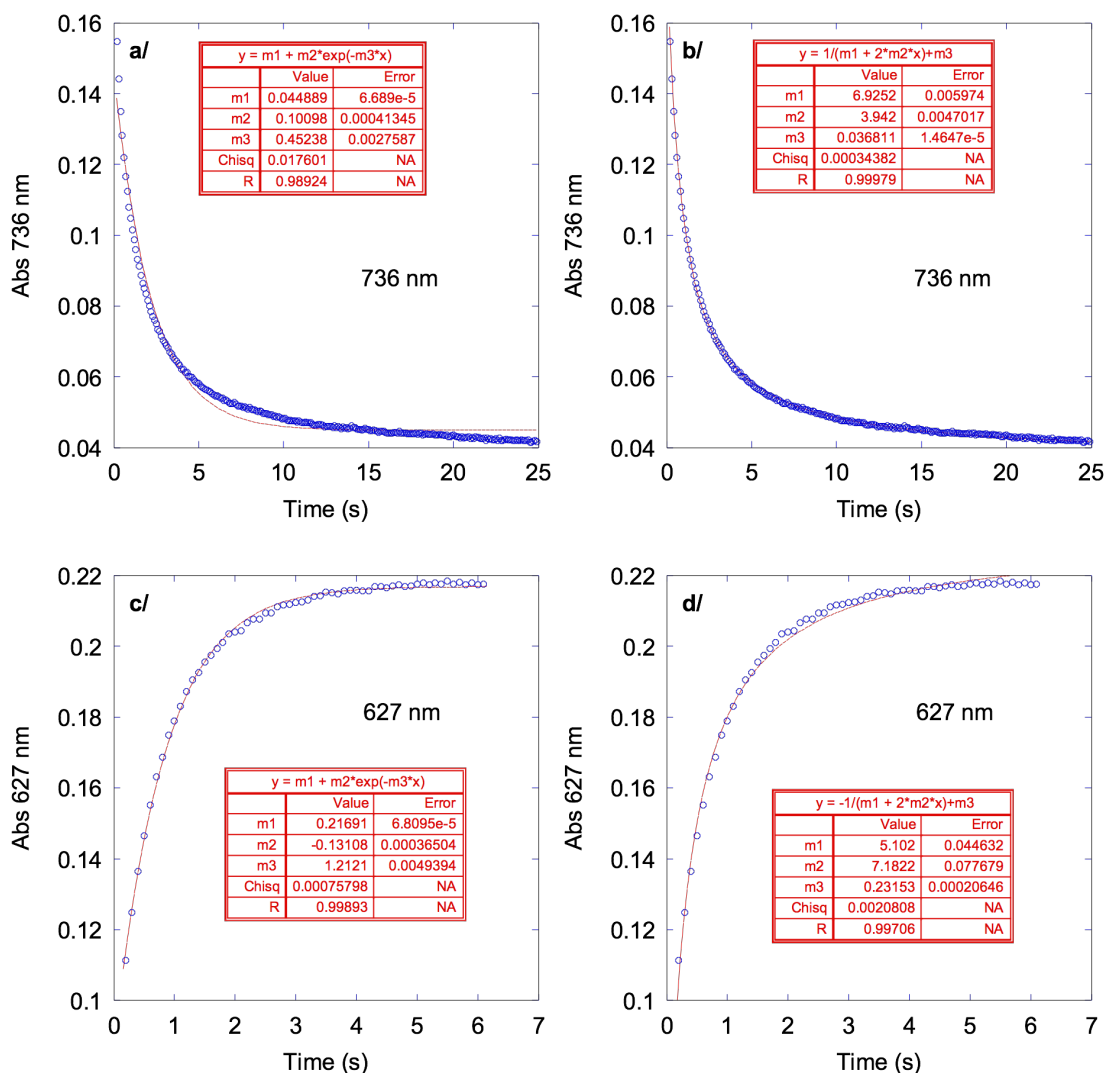


**Figure S34.** Experimental timetraces at 736 nm (a/ and b/, blue circles) recorded during the decay of the Fe<sup>IV</sup>O species and at 627 nm (c/ and d/, blue circles) during the growth of the Fe<sup>III</sup>(OPh) species after mixing a 1 mM solution of  $[(L_5^{PhOH})Fe^{II}(OTf)](OTf)$  (**4**) in MeCN containing 300 equiv. cyclooctene with 1.2 equiv. PhIO at 293 K and simulated timetraces (red lines) obtained by fitting the data to a monoexponential law (a/ and c/) and a 2<sup>nd</sup> order law (b/ and d/).

**Comment :** The decay of Fe<sup>IV</sup>O is best described by a bimolecular mechanism. In the presence of cyclooctene (300 equiv.), the  $[(L_5^{PhOH})Fe^{IV}(O)]^{2+}$  decay remains best fitted as a 2<sup>nd</sup> order decay (Figure S24), with the same decay rate ( $k = 2m_2 = 7.880 \pm 0.005 \text{ L}\cdot\text{mol}^{-1}\cdot\text{s}^{-1}$ ) as in the absence of cyclooctene. The main decay pathway thus remains the bimolecular reaction of Fe<sup>IV</sup>O. The direct attack of cyclooctene onto Fe<sup>IV</sup>O (which would lead to a 1<sup>st</sup> order decay of Fe<sup>IV</sup>O) only constitutes a minor one, in line with the modest conversion of PhIO (15.5 %, Table S1).

#### IV.2. Reaction of $[(L_5^{PhOH})Fe^{II}(OTf)](OTf)$ (**4**) with $H_2O_2$ .

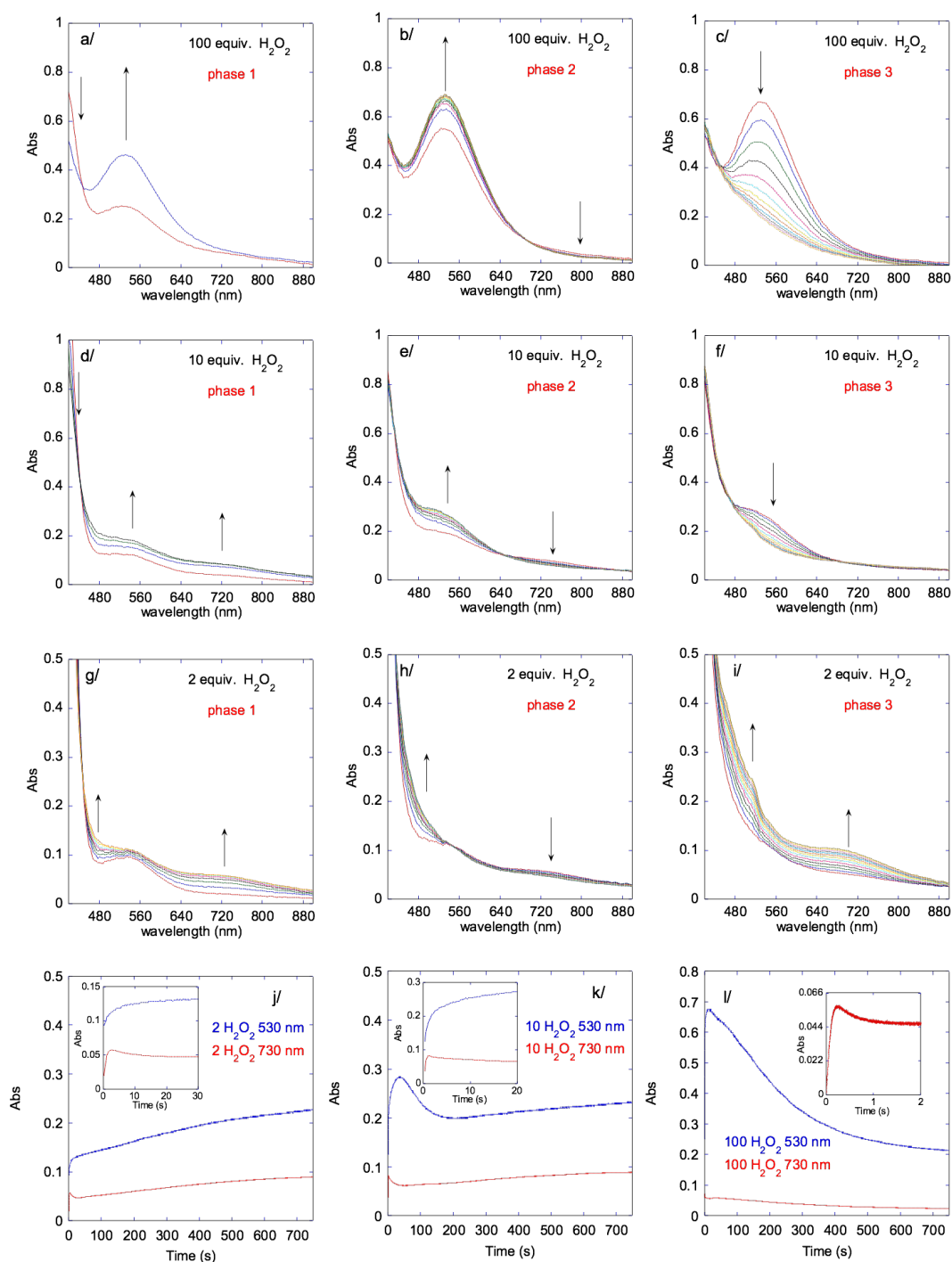


**Figure S35.** Evolution of the UV-vis spectrum of a solution of  $[(L_5^{PhOH})Fe^{II}(OTf)](OTf)$  (**4**) 1 mM in MeCN at 293 K upon addition of various amounts of  $H_2O_2$ . 100 equiv. (a/, b/ and c/), 10 equiv. (d/, e/ and f/), and 2 equiv. (g/, h/ and i/). Timetraces at 530 and 730 nm for x equiv.  $H_2O_2$  (x = 2 (j/), 10 (k/) or 100 (l/))

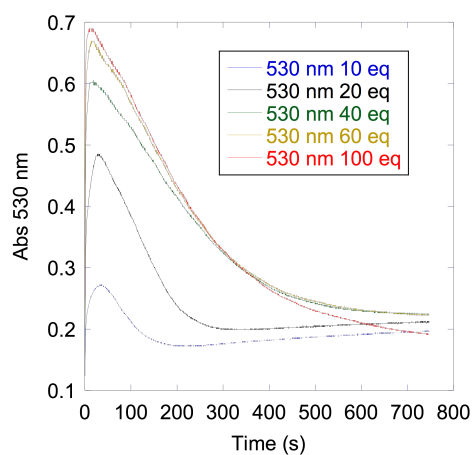


**Figure S36.** Formation and decay of  $\text{Fe}^{\text{III}}(\text{OOH})$  monitored at 530 nm observed upon mixing a solution of  $[(\text{L}_5^{\text{PhOH}})\text{Fe}^{\text{II}}(\text{OTf})](\text{OTf})$  1 mM in MeCN at 293 K and  $x$  equiv.  $\text{H}_2\text{O}_2$ ,  $x = 10, 20, 40, 60, 100$ .

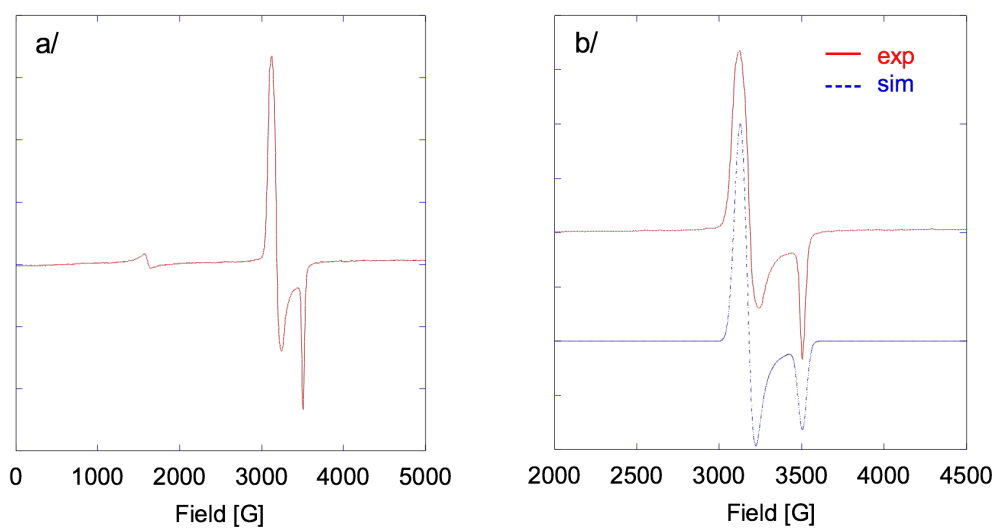


**Figure S37.** X band EPR spectrum in MeCN (90 K) of the solution obtained upon addition of 100 equiv.  $\text{H}_2\text{O}_2$  to a 2 mM solution of  $[(\text{L}_5^{\text{PhOH}})\text{Fe}^{\text{II}}(\text{OTf})](\text{OTf})$  (**4**) in MeCN at 293 K (full scale, a/) and simulated spectrum of the low spin signal with parameters  $g = 2.205 \ 2.165 \ 1.965$ .

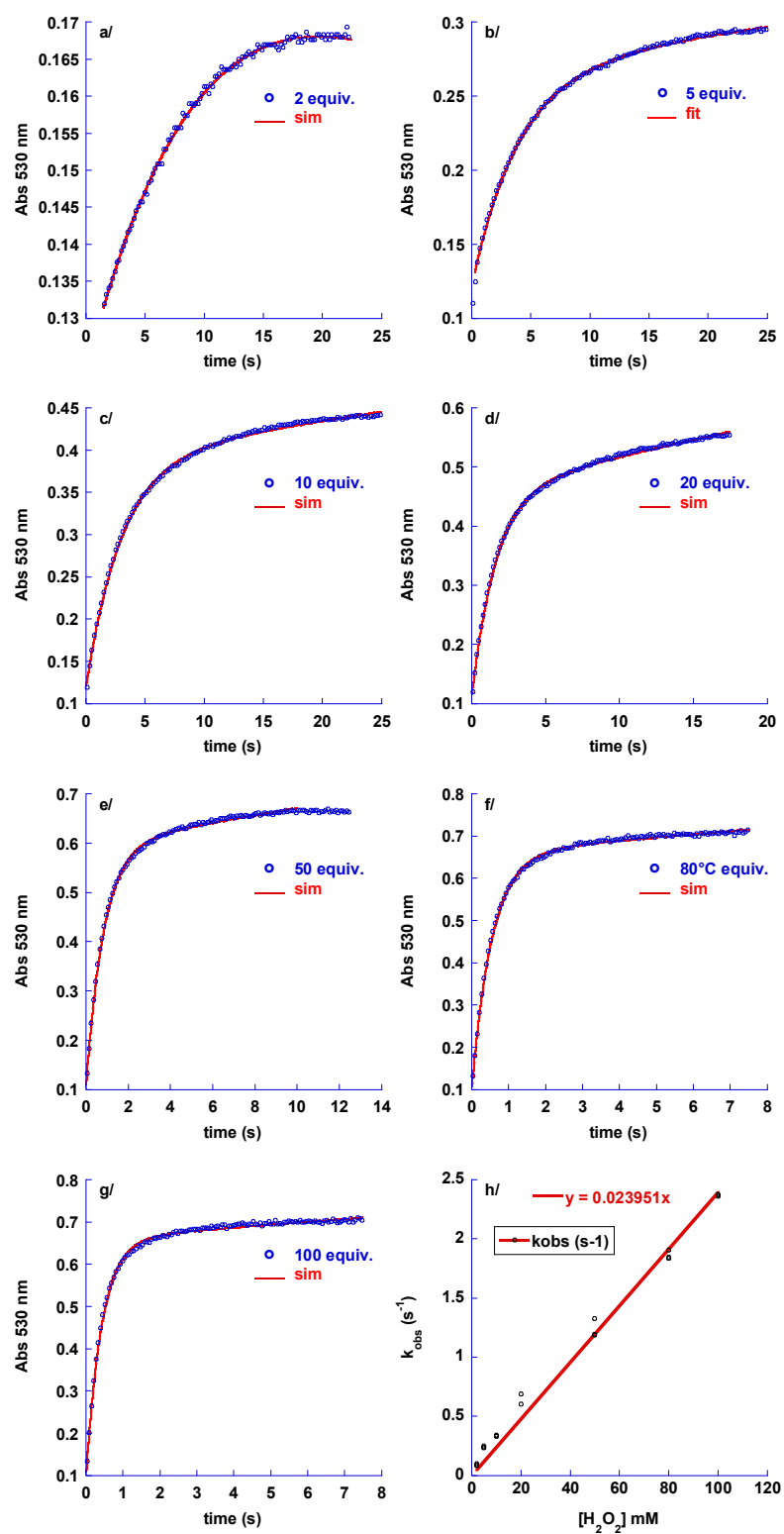


**Figure S38.** Timetraces of the growth of  $\text{Fe}^{\text{III}}(\text{OOH})$  monitored at 530 nm (a/ to g/, *experimental*: blue, *fitted*: red) in the UV-vis spectrum of the solution obtained upon addition of  $x$  equiv.  $\text{H}_2\text{O}_2$  to a 1 mM solution of  $[(\text{L}_5^{\text{PhOH}})\text{Fe}^{\text{II}}(\text{OTf})](\text{OTf})$  in MeCN at 293 K ( $x = 2, 5, 10, 50, 80, 100$  equiv.  $\text{H}_2\text{O}_2$ ). Curves were fitted at 530 nm to a monoexponential model  $\text{Abs} = a + b + c \cdot \exp(-kt)$ . The rate constants for the growth (h/) of the 530 nm chromophore are plotted as a function of  $[\text{H}_2\text{O}_2]$ .

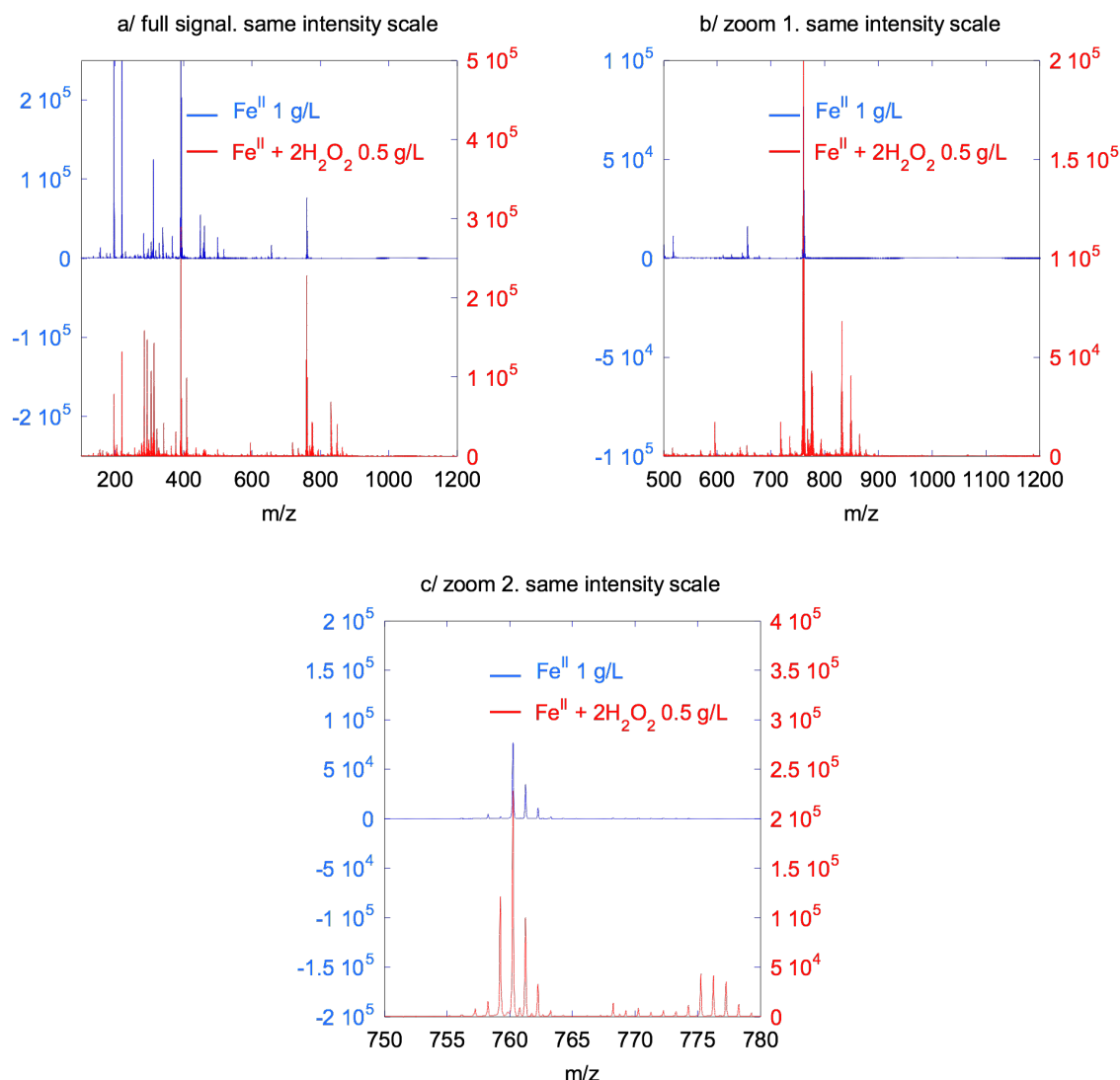


**Figure S39.** Comparison of HR-ESI-MS spectra of a  $[(L_5^{\text{PhOH}})\text{Fe}^{\text{II}}(\text{OTf})](\text{OTf})$  (**4**) 1 g/L solution and of a solution obtained by mixing the former  $[(L_5^{\text{PhOH}})\text{Fe}^{\text{II}}(\text{OTf})](\text{OTf})$  solution with 2 equiv.  $\text{H}_2\text{O}_2$  at 293 K (final iron concentration 0.5 g/L).

**Comment :** The masses below  $m/z = 400$  correspond to decomposition products in these concentrated conditions (a/). Above  $m/z = 400$  (b/ and c/), the spectrum of  $[(L_5^{\text{PhOH}})\text{Fe}^{\text{II}}(\text{OTf})](\text{OTf})$  alone is dominated by a peak at  $m/z = 760.2467$  assigned to  $[(L_5^{\text{PhOH}})\text{Fe}^{\text{II}}(\text{OTf})]^+$  (blue). In the presence of  $\text{H}_2\text{O}_2$ , the spectrum is dominated by peaks at  $m/z = 759.2500$  and  $760.2467$  assigned to  $[(L_5^{\text{PhO}^{\bullet}})\text{Fe}^{\text{II}}(\text{OTf})]^+$  and  $[(L_5^{\text{PhOH}})\text{Fe}^{\text{II}}(\text{OTf})]^+$  respectively ( $m/z$  calcd for  $[(L_5^{\text{PhOH}})\text{Fe}^{\text{II}}(\text{OTf})]^+$ : 760.2544, error = 10 ppm),  $m/z$  calcd for  $[(L_5^{\text{PhO}^{\bullet}})\text{Fe}^{\text{II}}(\text{OTf})]^+$ : 759.2466, error = 4.5 ppm). But a second group of peaks around  $m/z = 776$  is assigned to  $\text{Fe}^{\text{IV}}\text{O}$  species (see Figures S40-S42).

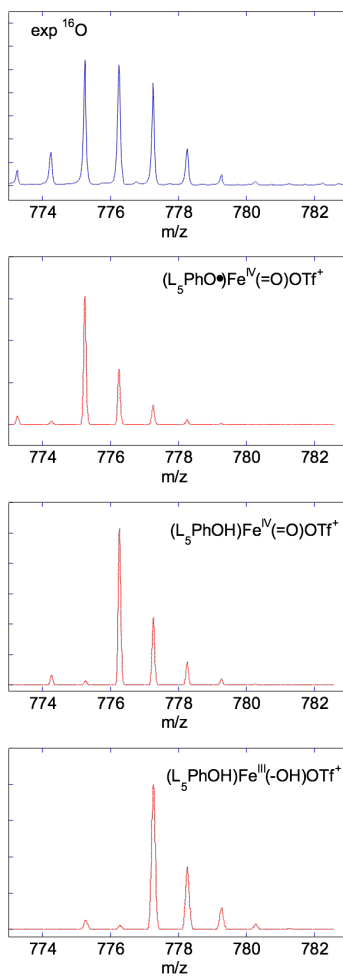


**Figure S40.** Zoom of the  $m/z = 776$  massif of the HR-ESI-MS spectrum recorded upon mixing  $[(L_5^{PhOH})Fe^{II}(OTf)](OTf)$  in MeCN with 2 equiv.  $H_2O_2$  at 293 K (top) and simulated spectra of different ions:  $[(L_5^{PhO^*})Fe^{IV}(O)(OTf)]^+$ : 775.2421,  $[(L_5^{PhOH})Fe^{IV}(O)(OTf)]^+$ : 776.2499,  $[(L_5^{PhOH})Fe^{III}(OH)(OTf)]^+$ : 777.2572.

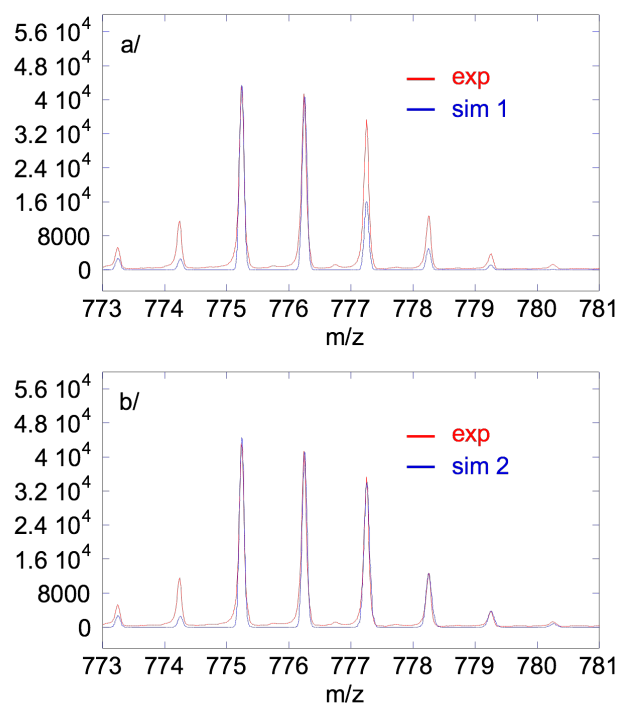


**Figure S41.** HR-ESI-MS spectrum (red) recorded upon mixing  $[(L_5^{\text{PhOH}})\text{Fe}^{\text{II}}(\text{OTf})](\text{OTf})$  in MeCN with 2 equiv.  $\text{H}_2\text{O}_2$  at 293 K and simulations (blue).

**Comment :** The massif corresponds to the overlay of the patterns of several ions. The peaks at  $m/z = 775.2414$  and  $776.2525$  can be reproduced by simulation (sim 1, a/) as the sum of the isotopic patterns of two components:  $m/z$  calcd for  $[(L_5^{\text{PhOH}})\text{Fe}^{\text{IV}}(\text{O})(\text{OTf})]^+$ : 776.2499, error = 3.3 ppm,  $m/z$  calcd for  $[(L_5^{\text{PhO}^\bullet})\text{Fe}^{\text{IV}}(\text{O})(\text{OTf})]^+$ : 775.2421, error = 0.9 ppm. However, a third component must be added to properly simulate the full pattern and the intensity of the peak at  $m/z = 777.2529$  (sim 2, b/):  $m/z$  calcd for  $[(L_5^{\text{PhOH}})\text{Fe}^{\text{III}}(\text{OH})(\text{OTf})]^+$ : 777.2572, error = 5.5 ppm. The overall pattern corresponds to a combination of the two  $\text{Fe}^{\text{IV}}\text{O}$  ions and an  $\text{Fe}^{\text{III}}(\text{OH})$  decay product.

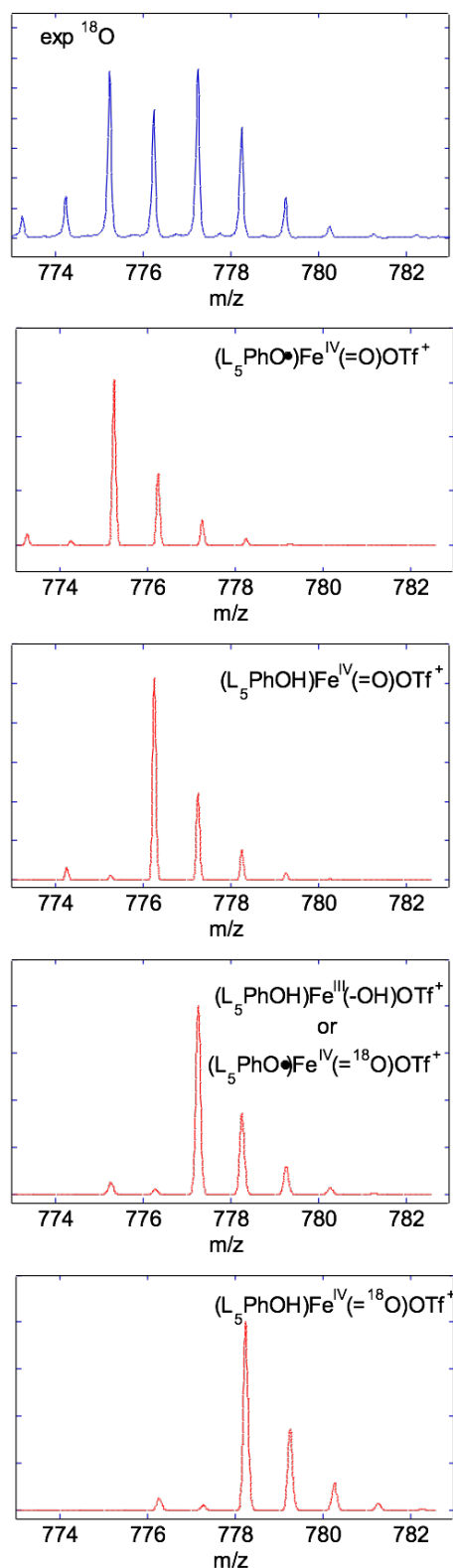


**Figure S42.** Zoom on the  $m/z = 776$  massif of the HR-ESI-MS spectrum recorded upon mixing  $[(L_5^{PhOH})Fe^{II}(OTf)](OTf)$  in MeCN with 2 equiv.  $H_2^{18}O_2$  at 293 K (top) and simulated spectra of different ions:  $[(L_5^{PhO})Fe^{IV}(O)(OTf)]^+$ : 775.2421,  $[(L_5^{PhOH})Fe^{IV}(O)(OTf)]^+$ : 776.2499,  $[(L_5^{PhOH})Fe^{III}(OH)(OTf)]^+$ : 777.2572  $[(L_5^{PhOH})Fe^{IV}(^{18}O)(OTf)]^+$ : 778.2536. Note that  $[(L_5^{PhO})Fe^{IV}(^{18}O)(OTf)]^+$  ( $m/z = 777.2468$ ) cannot be distinguished from  $[(L_5^{PhOH})Fe^{III}(OH)(OTf)]^+$  by simulation.

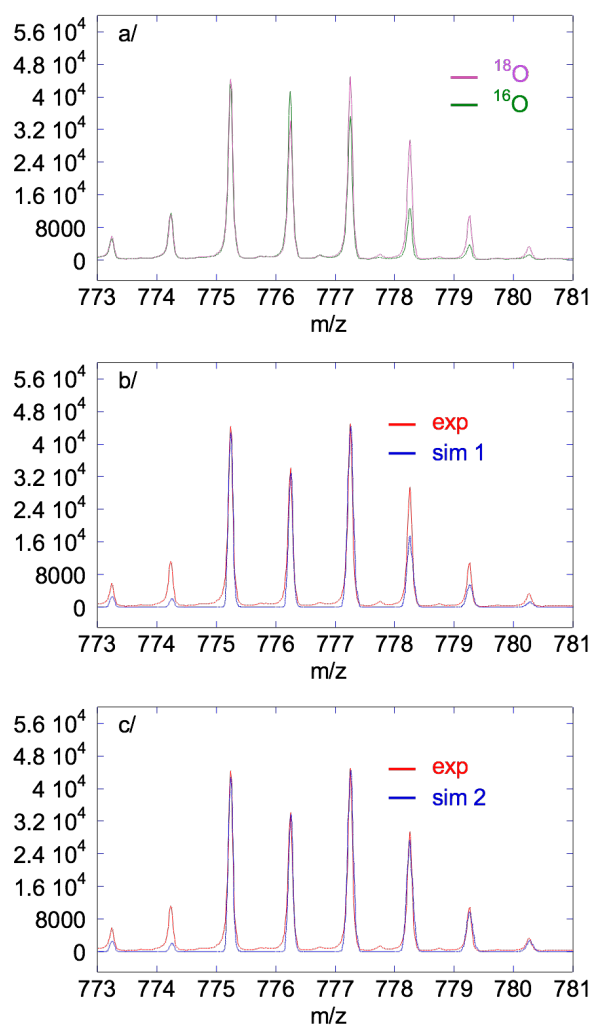


**Figure S43.** HR-ESI-MS spectrum recorded upon mixing  $[(L_5^{\text{PhOH}})\text{Fe}^{\text{II}}(\text{OTf})](\text{OTf})$  in MeCN with 2 equiv.  $\text{H}_2^{18}\text{O}_2$  at 293 K. a/ Comparison with the  $\text{H}_2^{16}\text{O}_2$  experiment. b/ Experimental (red) vs simulated spectrum (blue) considering only three components:  $[(L_5^{\text{PhOH}})\text{Fe}^{\text{IV}}(\text{O})(\text{OTf})]^+$ :  $m/z = 776.2499$ ,  $[(L_5^{\text{PhO}^*})\text{Fe}^{\text{IV}}(\text{O})(\text{OTf})]^+$ :  $m/z = 775.2421$ , and  $[(L_5^{\text{PhOH}})\text{Fe}^{\text{III}}(\text{OH})(\text{OTf})]^+$ :  $m/z = 777.2572$ . The intensity at  $m/z = 778.2549$  and  $779.2586$  cannot be reproduced. c/ Experimental (red) vs simulated spectrum (blue) considering a fourth component, allowing to properly simulate the mass:  $(L_5^{\text{PhOH}})\text{Fe}^{\text{IV}}(^{18}\text{O})\text{OTf}^+$ .  $m/z$  calcd for  $(L_5^{\text{PhOH}})\text{Fe}^{\text{IV}}(^{18}\text{O})\text{OTf}^+$ :  $778.2536$ , error = 1.6 ppm). Note: a) the solvents were not dried, hence the presence of <sup>16</sup>O species at  $m/z = 775, 776$  and  $777$ , b) The peak at  $m/z = 777$  can be assigned either to  $(L_5^{\text{PhOH}})\text{Fe}^{\text{III}}(\text{OH})\text{OTf}^+$  ( $m/z = 777.2572$ ) or to  $(L_5^{\text{PhO}^*})\text{Fe}^{\text{IV}}(^{18}\text{O})\text{OTf}^+$  ( $m/z = 777.2468$ ) The ion masses are too close to be distinguished by simulation.

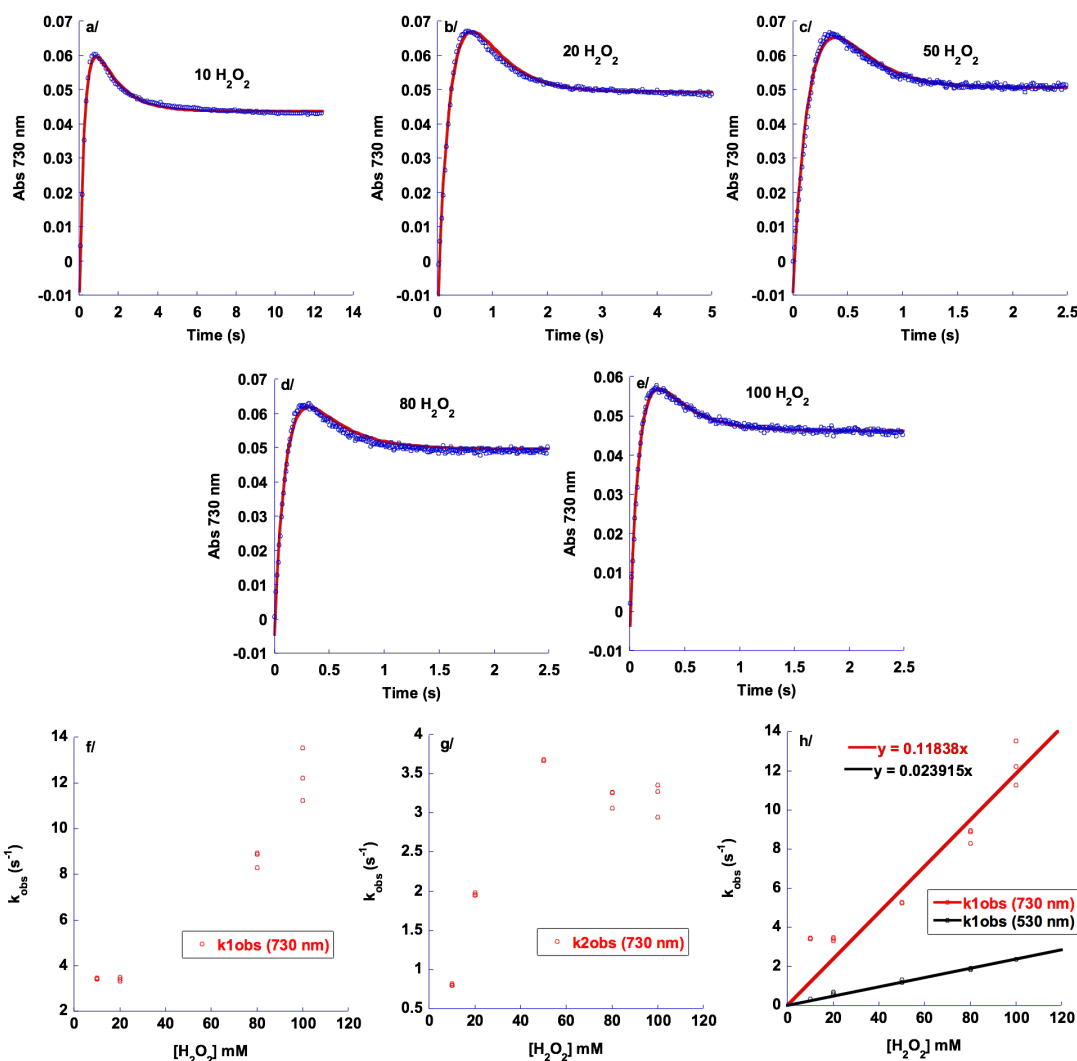


**Figure S44.** Timetraces at 730 nm (a/ to e/, *experimental*: blue, *fitted*: red) of the UV-vis spectrum of the solution obtained upon addition of  $x$  equiv.  $\text{H}_2\text{O}_2$  to a 1 mM solution of  $[(\text{L}_5^{\text{PhOH}})\text{Fe}^{\text{II}}(\text{OTf})](\text{OTf})$  (**4**) in MeCN at 293 K ( $x = 10, 20, 50, 80, 100$  equiv.  $\text{H}_2\text{O}_2$ ). Curves were fitted at 730 nm to a biexponential model  $y = a + b \cdot \exp(-k_{1\text{obs}}t) + c \cdot \exp(-k_{2\text{obs}}t)$ . The rate constants for the growth (f/) and decay (g/) of the 730 nm chromophore are plotted as a function of  $[\text{H}_2\text{O}_2]$ . (h/) Comparison of the rate constants for the growth of  $\text{Fe}^{\text{IV}}\text{O}$  ( $k_{1\text{obs}}(730 \text{ nm})$ ) and  $\text{Fe}^{\text{III}}(\text{OOH})$  ( $k_{1\text{obs}}(530 \text{ nm})$ ).

**Comment :**  $k_{1\text{obs}}(730 \text{ nm})$  shows a linear dependence on  $[\text{H}_2\text{O}_2]$  above 20 equiv.  $\text{H}_2\text{O}_2$  (pseudo 1<sup>st</sup> order conditions), which is in line with an associative process between (**4**) and  $[\text{H}_2\text{O}_2]$ . The  $\text{Fe}^{\text{IV}}\text{O}$  decay rate  $k_{2\text{obs}}(730 \text{ nm})$  shows a linear  $[\text{H}_2\text{O}_2]$  dependence up to 50 mM  $\text{H}_2\text{O}_2$  ( $k_2 = 77 \text{ L} \cdot \text{mol}^{-1} \cdot \text{s}^{-1}$ ), before decreasing when concentrations above 50 mM  $\text{H}_2\text{O}_2$  were used: at high  $[\text{H}_2\text{O}_2]$ ,  $\text{Fe}^{\text{III}}(\text{OOH})$  becomes predominant and the absorption of this chromophore at 730 nm cannot be neglected. As the amount of  $\text{Fe}^{\text{III}}(\text{OOH})$  increases during the decay of  $\text{Fe}^{\text{IV}}\text{O}$  above 50 mM,  $k_{2\text{obs}}(730 \text{ nm})$  becomes a composite of  $\text{Fe}^{\text{III}}(\text{OOH})$  formation and  $\text{Fe}^{\text{IV}}\text{O}$  decay, hence the deviation from the linear regime.

**Note:** In the  $A \rightarrow B \rightarrow C$  model ( $A = \text{Fe}^{\text{II}}$ ,  $B = \text{Fe}^{\text{IV}}\text{O}$ ,  $C = \text{decay product}$ ),  $[A] = A_0 e^{-k_{1\text{obs}}t}$ ,  $[B] = A_0 k_{1\text{obs}} (e^{-k_{1\text{obs}}t} - e^{-k_{2\text{obs}}t}) / (k_{2\text{obs}} - k_{1\text{obs}})$ ,  $[C] = A_0 [1 - (k_{2\text{obs}} e^{-k_{1\text{obs}}t} - k_{1\text{obs}} e^{-k_{2\text{obs}}t}) / (k_{2\text{obs}} - k_{1\text{obs}})]$ , with  $A_0$  being the initial concentration of A, and  $k_{1\text{obs}}$  and  $k_{2\text{obs}}$  the rate constants for  $A \rightarrow B$  and  $B \rightarrow C$  respectively. The absorbance is thus  $\text{Abs} = \varepsilon_A A_0 + A_0 \exp(-k_{1\text{obs}}t) * [k_{1\text{obs}}(\varepsilon_B - \varepsilon_C) + k_{2\text{obs}}(\varepsilon_A - \varepsilon_C)] / (k_{2\text{obs}} - k_{1\text{obs}}) + A_0 \exp(-k_{2\text{obs}}t) * [k_{2\text{obs}}\varepsilon_C - k_{1\text{obs}}\varepsilon_B] / (k_{2\text{obs}} - k_{1\text{obs}})$ .

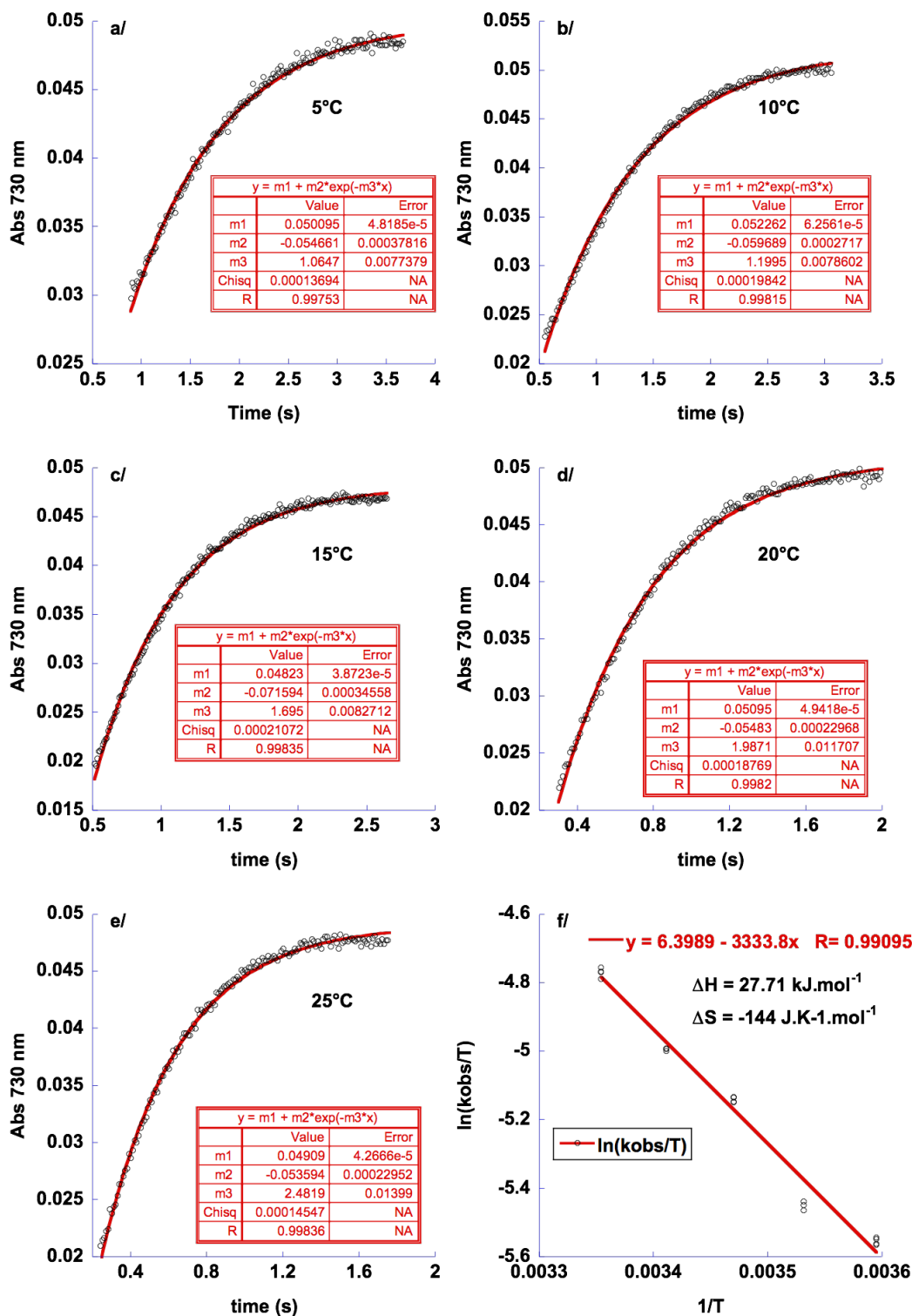


**Figure S45.** Time traces of the absorbance of the Fe<sup>IV</sup>O chromophore (730 nm) at various temperatures (5, 10, 15, 20, 25 °C) upon addition of 2 equiv. H<sub>2</sub>O<sub>2</sub> to a solution of [(L<sub>5</sub><sup>PhOH</sup>)Fe<sup>II</sup>(OTf)](OTf) 1 mM in MeCN (a/e) and monoexponential fit at 730 nm. Eyring plot for the Fe<sup>IV</sup>O (f). Extracted parameters:  $\Delta H_{1obs}^\ddagger = 27.7 \pm 1.4 \text{ kJ}\cdot\text{mol}^{-1}$ ;  $\Delta S_{1obs}^\ddagger = -144 \pm 4.7 \text{ J}\cdot\text{K}^{-1}\cdot\text{mol}^{-1}$ .

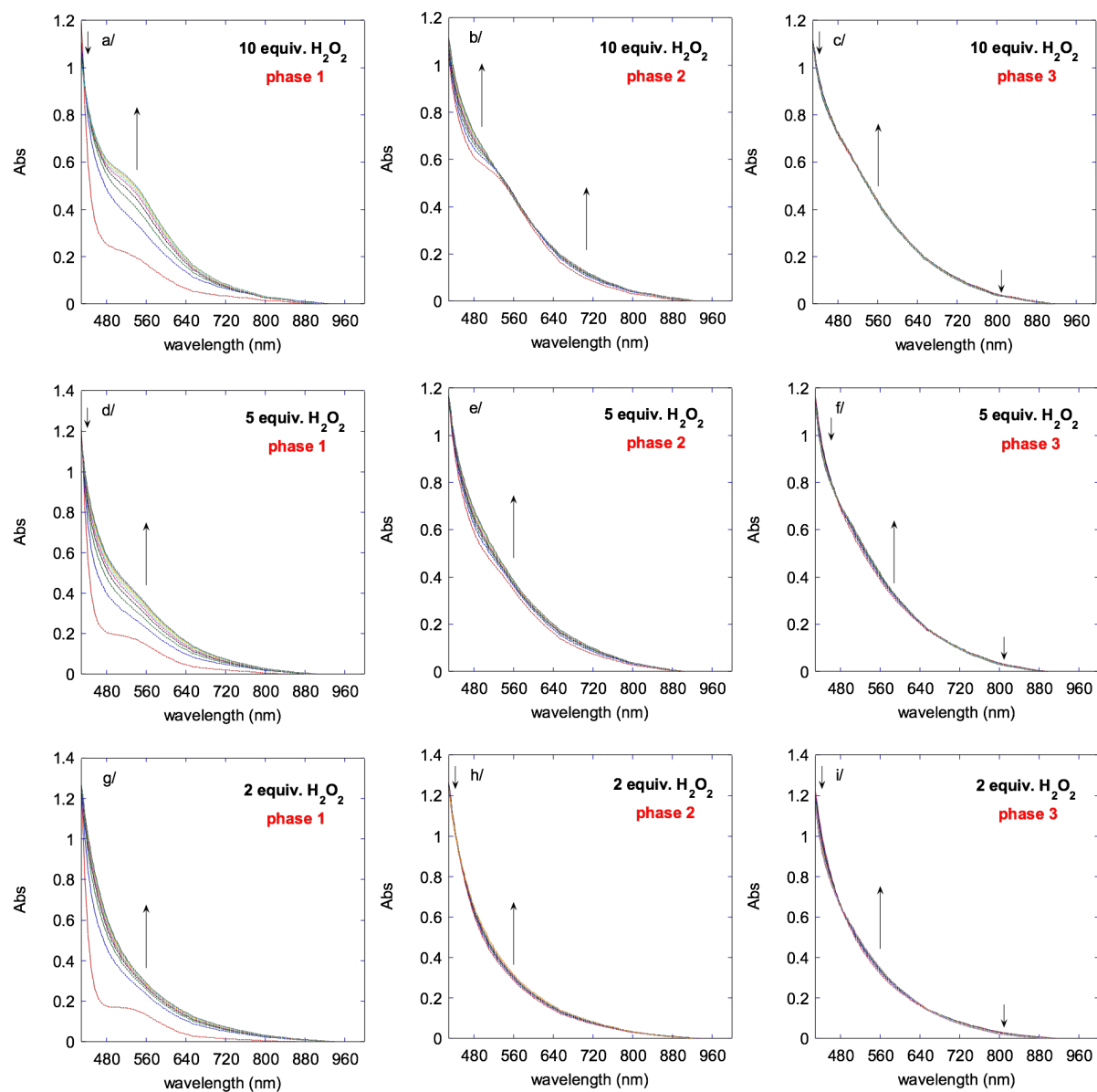


**Figure S46.** Evolution of the UV-vis spectrum of a solution of  $[(L_5)Fe^{II}(OTf)](OTf)$  1 mM in MeCN at 293 K upon addition of various amounts of  $H_2O_2$ . 10 equiv. (a/, b/ and c/), 5 equiv. (d/, e/ and f/), and 2 equiv. (g/, h/ and i/).

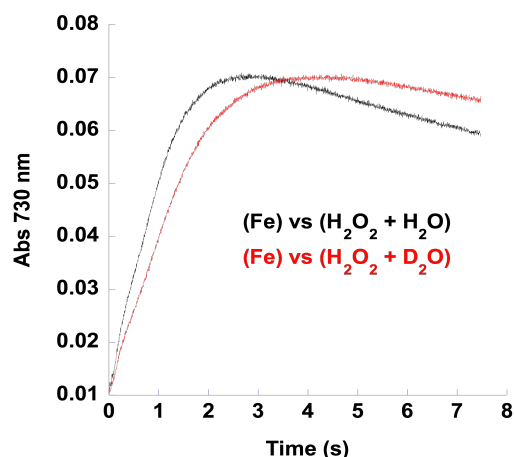


**Figure S47.** Timetraces of the absorbance at 730 nm upon mixing 150  $\mu\text{L}$  of a solution **A** (2 mM  $[(\text{L}_5^{\text{PhOH}})\text{Fe}^{\text{II}}(\text{OTf})](\text{OTf})$  in neat MeCN) and 150  $\mu\text{L}$  of solution **B** (4 mM  $\text{H}_2\text{O}_2$  solution in either MeCN/ $\text{H}_2\text{O}$  (96:4) (black line) or MeCN/ $\text{D}_2\text{O}$  (96:4) (red line)).

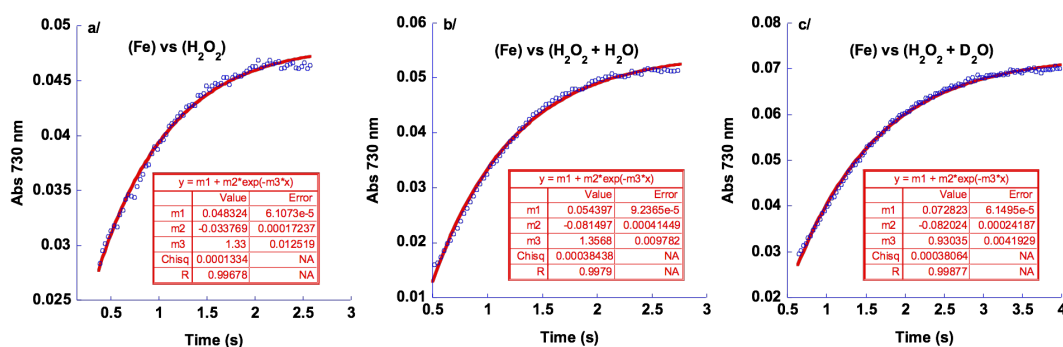


**Figure S48.** Experimental (blue dots) and fitted (red plain line) timetraces of the absorbance at 730 nm upon mixing 150  $\mu\text{L}$  of solutions **A** containing  $[(\text{L}_5^{\text{PhOH}})\text{Fe}^{\text{II}}(\text{OTf})](\text{OTf})$  2 mM and 150  $\mu\text{L}$  of solution **B** containing  $\text{H}_2\text{O}_2$  4 mM. (**B**) was prepared in (a/) neat MeCN, (b/) MeCN/ $\text{H}_2\text{O}$  96:4 v:v, or (c/) MeCN/ $\text{D}_2\text{O}$  96:4 v:v. Experimental data (growth of  $\text{Fe}^{\text{IV}}\text{O}$ ) was fitted to a monoexponential law.

**Table S2.** Rate constants (in  $\text{s}^{-1}$ ) extracted from the monoexponential fit of the growth of the absorbance at 730 nm, upon mixing equal volumes of solution (**A**)  $[(\text{L}_5^{\text{PhOH}})\text{Fe}^{\text{II}}(\text{OTf})](\text{OTf})$  2 mM and solution (**B**)  $\text{H}_2\text{O}_2$  4 mM. (**B**) was either prepared in neat MeCN, MeCN/ $\text{H}_2\text{O}$  96:4 v:v, or MeCN/ $\text{D}_2\text{O}$  96:4 v:v. Values are the average of three runs.

$\text{H}_2\text{O}_2$ solution in	$k_{\text{obs}}$ ( $\text{s}^{-1}$ )
neat MeCN	$1.27 \pm 0.05$
MeCN/ $\text{H}_2\text{O}$ 96:4	$1.35 \pm 0.04$
MeCN/ $\text{D}_2\text{O}$ 96:4	$0.97 \pm 0.03$

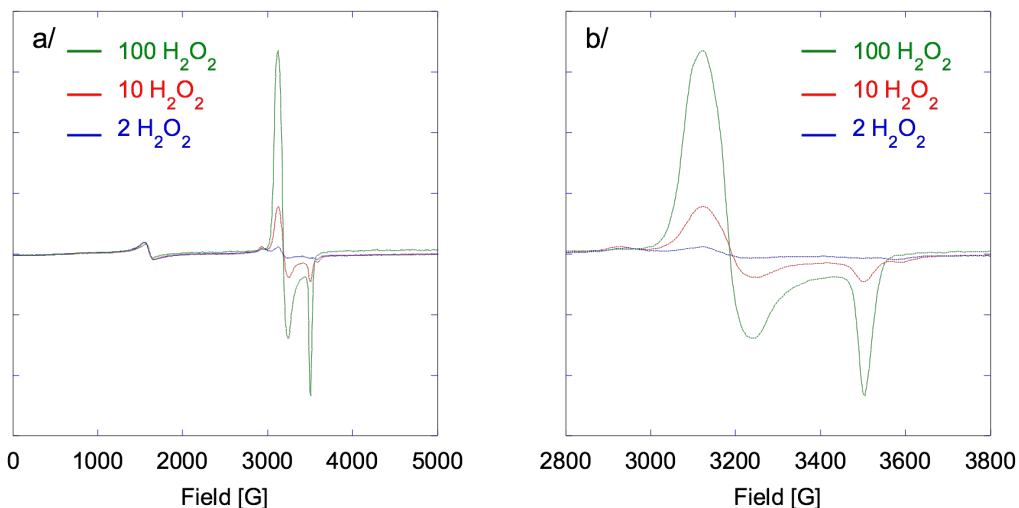


**Figure S49.** X band EPR spectra in MeCN (90 K) of the solution obtained upon addition of  $x$  equiv.  $\text{H}_2\text{O}_2$  ( $x = 2, 10$  or  $100$ ) to a 2 mM solution of  $[(\text{L}_5^{\text{PhOH}})\text{Fe}^{\text{II}}(\text{OTf})](\text{OTf})$  at 293 K (full scale, a/) and low spin region (b/).

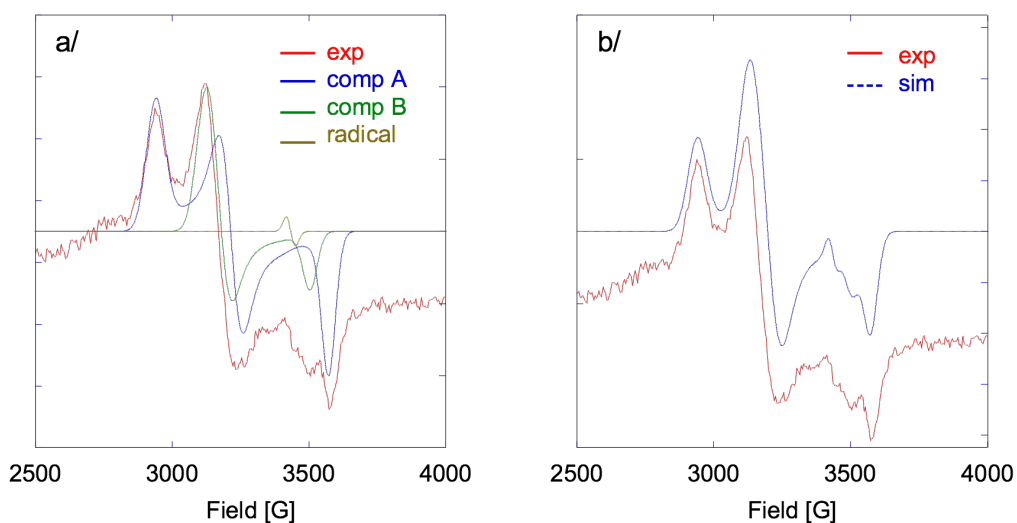


**Figure S50.** X band EPR spectra in MeCN (90 K) of the solution obtained upon addition of 2 equiv.  $\text{H}_2\text{O}_2$  to a 2 mM solution of  $[(\text{L}_5^{\text{PhOH}})\text{Fe}^{\text{III}}(\text{OTf})](\text{OTf})$  in MeCN at 293 K (red, low spin region) and simulated spectra: isolated components (a/) and summed spectrum of the 3 components (b/). *Component A*:  $g = 2.34 \ 2.14 \ 1.928$ ; *Component B*:  $g = 2.205 \ 2.165 \ 1.965$ ; *radical*:  $g = 2.004$ . *Component A* is ascribed to an  $\text{Fe}^{\text{III}}(\text{OH})$  species, likely to correspond to  $(\text{N}_5)\text{Fe}^{\text{III}}(\text{OH})^{2+}$  and *Component B* to  $(\text{N}_4)\text{Fe}^{\text{III}}(\text{OOH})(\text{MeCN})^{2+}$ . Simulation gives the ratio  $A / B : 0.8 / 1$ .

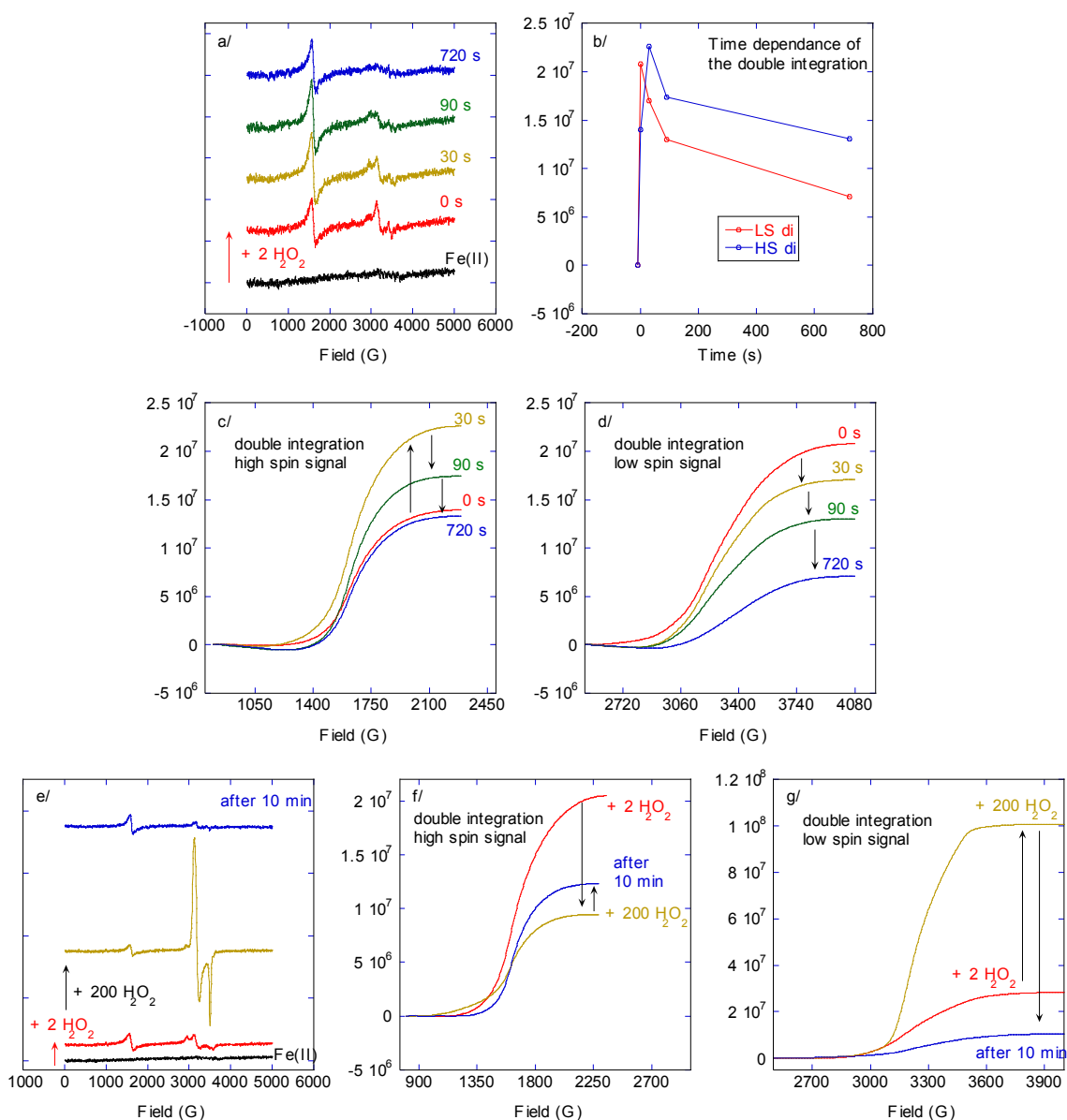


**Figure S51.** X band EPR spectra in MeCN (90 K) of the solution obtained upon addition of 2 equiv.  $\text{H}_2\text{O}_2$  to a 2 mM solution of  $[(\text{L}_5^{\text{PhOH}})\text{Fe}^{\text{II}}(\text{OTf})](\text{OTf})$  (**4**) in MeCN at 293 K and its evolution (a/) and time dependence of the double integration of the signals (b/, c/ and d/). Spectra obtained upon addition of 2 equiv.  $\text{H}_2\text{O}_2$  to a 2 mM solution of (**4**) in MeCN at 293 K followed by addition of 200 extra equiv.  $\text{H}_2\text{O}_2$  (e/) and evolution of the double integration of the signals (f/ and g/).

**Comment :** The time dependence of the double integration of the signals in the presence of only 2 equiv.  $\text{H}_2\text{O}_2$  (b/) shows a monotonic decay of the low spin signals (d/) while the high spin ones first increase before decreasing (c/). The overall double integration remains very small throughout the experiment, in line with the conversion of  $\text{Fe}^{\text{II}}$  (diamagnetic) to  $\text{Fe}^{\text{IV}}\text{O}$  (EPR silent) followed by the conversion of  $\text{Fe}^{\text{IV}}\text{O}$  to  $\text{Fe}^{\text{III}}\text{-O-Fe}^{\text{III}}$  antiferromagnetically coupled dimers (EPR silent). The evolution of the high spin double integration (c/) suggest that  $\text{Fe}^{\text{IV}}\text{O}$  first decays to give a high spin  $\text{Fe}^{\text{III}}$  species, which then converts to the O-bridged dimers as thermodynamic sink.

For comparison purposes, a second experiment (e/ f/ and g/) shows the evolution of the spectrum upon addition of 2 equiv.  $\text{H}_2\text{O}_2$  to a 2 mM solution of  $[(\text{L}_5^{\text{PhOH}})\text{Fe}^{\text{II}}(\text{OTf})](\text{OTf})$  in MeCN at 293 K

followed by addition of 200 extra equiv.  $\text{H}_2\text{O}_2$ , and displays a significantly more intense signal, with a *circa* 90% conversion of  $\text{Fe}^{\text{II}}$  to LS  $\text{Fe}^{\text{III}}(\text{OOH})$  in the presence of excess  $\text{H}_2\text{O}_2$ .

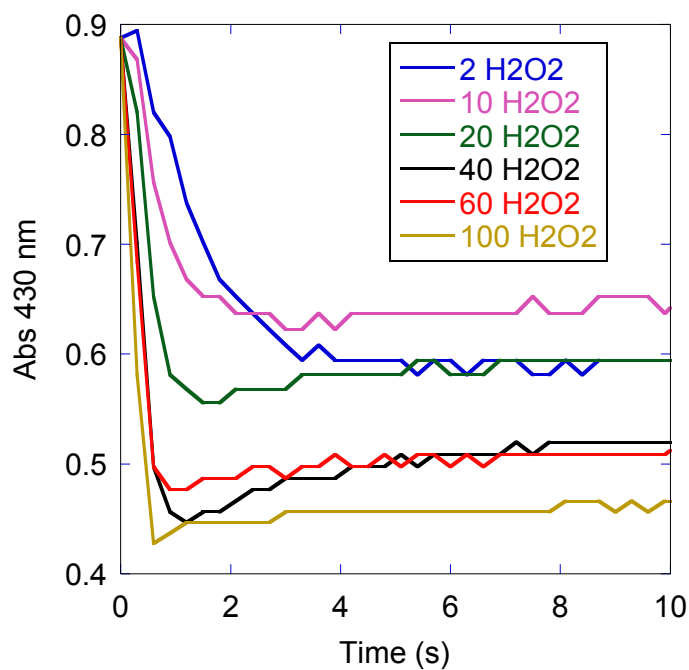


**Figure S52.** Timetraces at 430 nm (tail of the MLCT of  $[(\text{L}_5^{\text{PhOH}})\text{Fe}^{\text{II}}(\text{OTf})](\text{OTf})$ ) upon adding different amounts of  $\text{H}_2\text{O}_2$  to a 1 mM solution of  $[(\text{L}_5^{\text{PhOH}})\text{Fe}^{\text{II}}(\text{OTf})](\text{OTf})$  in MeCN at 293 K, indicating that a significant amount of  $\text{Fe}^{\text{II}}$  remains for 2 equiv.  $\text{H}_2\text{O}_2$  added at the maximum of  $\text{Fe}^{\text{IV}}\text{O}$  accumulation ( $t = 2\text{s}$ ).

**Table S3.** Crystallographic data and structure refinement details.

Compound	$[(L_5^{PhOH})Fe^{II}(H_2O)(OH)](PF_6)$ (5)	$[(L_5^{PhOH})Fe^{II}Cl](PF_6)$ (2)
CCDC	1992915	1992916
Empirical Formula	$(C_{33}H_{48}FeN_7O_3)$ , $(F_6P)$ , $(C_5H_{12}O)$ , $1/4(CO)$	$(C_{33}H_{45}ClFeN_7O)$ , $(F_6P)$ , $(CH_2Cl_2)$
$M_r$	893.75	876.96
Crystal size, mm <sup>3</sup>	0.220 x 0.160 x 0.030	0.140 x 0.050 x 0.030
Crystal system	monoclinic	monoclinic
Space group	$C2/c$	$P2_1/c$
a, Å	41.523(2)	15.0611(14)
b, Å	10.7009(5)	27.640(2)
c, Å	21.0891(10)	9.9365(7)
$\alpha$ , °	90	90
$\beta$ , °	100.475(2)	106.973(5)
$\gamma$ , °	90	90
Cell volume, Å <sup>3</sup>	9214.4(8)	3956.2(6)
Z ; Z'	8 ; 1	4 ; 1
T, K	100 (1)	100(1)
Radiation type ;	MoK $\alpha$ ; 0.71073	MoK $\alpha$ ; 0.71073
$F_{000}$	3 768	1816
$\mu$ , mm <sup>-1</sup>	0.432	0.691
range, °	1.964 - 30.586	1.414 - 30.599
Reflection collected	101 577	93 463
Reflections unique	14 074	12 050
$R_{int}$	0.1315	0.2854
GOF	1.053	0.975
Refl. obs. ( $I > 2\sigma(I)$ )	8 852	4491
Parameters	541	516
wR <sub>2</sub> (all data)	0.2758	0.2410
R value ( $I > \sigma_2(I)$ )	0.0853	0.0854
Largest diff. peak and (shift/ $\sigma$ )max	1.769 ; -0.872	0.912 ; -0.898
	0.003	0.000

- [1] G. M. Sheldrick, University of Göttingen, Germany, Göttingen, **1997**.
- [2] G. M. Sheldrick, *Acta Crystallogr., Sect. A: Found. Crystallogr.* **2008**, *64* 112-122.
- [3] L. J. Farrugia, *J. Appl. Cryst.* **1999**, *32*, 837.
- [4] J. Pérez-Prieto, R. Eugenia Galian, P. Oña Burgos, M. d. C. Morant Miñana, M. A. Miranda, F. López-Ortiz, *Org. Lett.* **2005**, *7*, 3869-3872.
- [5] X. Wang, A. Thevenon, J. L. Brosmer, I. Yu, S. I. Khan, P. Mehrkhodavandi, P. L. Diaconescu, *J Am Chem Soc.* **2014**, *136*, 11264-11267.
- [6] L. Xu, I. A. Setyawati, J. Pierrero, M. Pink, V. G. Young, B. O. Patrick, S. J. Rettig, C. Orvig, *Inorg. Chem.* **2000**, *39*, 5958-5963.
- [7] C. Baffert, M.-N. Collomb, A. Deronzier, S. Kjaergaard-Knudsen, J.-M. Latour, K. H. Lund, C. J. McKenzie, M. Mortensen, L. P. Nielsen, N. Thorup, *Dalton Transactions* **2003**, 1765-1772.
- [8] N. Ségaud, J.-N. Rebilly, K. Sénéchal-David, R. Guillot, L. Billon, J.-P. Baltaze, J. Farjon, O. Reinaud, F. Banse, *Inorg. Chem.* **2013**, *52*, 691-700.
- [9] D. F. Evans, *Journal of the Chemical Society (Resumed)* **1959**, 2003-2005.
- [10] G. A. Bain, J. F. Berry, *J. Chem. Educ.* **2008**, *85*, 532.
- [11] J.-N. Rebilly, W. Zhang, C. Herrero, H. Dridi, K. Sénéchal-David, R. Guillot, F. Banse, *Chem. Eur. J.* **2020**, *26*, 659-668.